Cellular and Molecular Neurobiology
https://doi.org/10.1007/s10571-020-00787-5

ORIGINAL RESEARCH

A Balancing Act: The Immune System Supports Neurodegeneration and Neurogenesis

Paula Grazielle Chaves da Silva[1,2] · Kelly Hsu[2] · Jeanne L. Benton[2] · Barbara S. Beltz[2] · Silvana Allodi[1]

Received: 5 September 2019 / Accepted: 4 January 2020

Abstract

Decapod crustaceans, like mammals, retain the ability to make new neurons throughout life. In mammals, immune cells are closely associated with stem cells that generate adult-born neurons. In crayfish, evidence suggests that immune cells (hemocytes) originating in the immune system travel to neurogenic regions and transform into neural progenitor cells. This nontraditional immune activity takes place continuously under normal physiological conditions, but little is known under pathological conditions (neurodegeneration). In this study, the immune system and its relationship with neurogenesis were investigated during neurodegeneration (unilateral antennular ablation) in adult crayfish. Our experiments show that after ablation (1) Proliferating cells decrease in neurogenic areas of the adult crayfish brain; (2) The immune response, but not neurogenesis, is ablation-side dependent; (3) Inducible nitric oxide synthase (iNOS) plays a crucial role in the neurogenic niche containing neural progenitors during the immune response; (4) Brain areas targeted by antennular projections respond acutely (15 min) to the lesion, increasing the number of local immune cells; (5) Immune cells are recruited to the area surrounding the ipsilateral neurogenic niche; and (6) The vasculature in the niche responds acutely by dilation and possibly also neovascularization. We conclude that immune cells are important in both neurodegeneration and neurogenesis by contributing in physiological conditions to the maintenance of the number of neural precursor cells in the neurogenic niche (neurogenesis), and in pathological conditions (neurodegeneration) by coordinating NO release and vascular responses associated with the neurogenic niche. Our data suggest that neural damage and recovery participate in a balance between these competing immune cell roles.

Keywords Neurogenic niche · Immune response · Nitric oxide synthase · Hemocytes · Vasculature · Crayfish

Abbreviations

AL	Accessory lobe
APC	Anterior proliferation center
BrdU	Bromodeoxyuridine
CL9	Cluster 9
CL10	Cluster 10
CL16	Cluster 16
EDTA	Ethylenediaminetetraacetic acid
eNOS	Endothelial nitric oxide synthase
FITC	Fluorescein isothiocyanate
GS	Glutamine synthetase
HPT	Hematopoietic tissue
iNOS	Inducible nitric oxide synthase
LAN	Lateral antennular neuropil
MAN	Medial antennular neuropil
NO	Nitric oxide
NOS	Nitric oxide synthase
nNOS	Neuronal nitric oxide synthase
uNOS	Universal nitric oxide synthase
OL	Olfactory lobe
PB	Phosphate buffer
PBTx	PB with Triton X-100
PI	Propidium iodide

Barbara S. Beltz and Silvana Allodi have contributed equally to this work.

Electronic supplementary material The online version of this article (https://doi.org/10.1007/s10571-020-00787-5) contains supplementary material, which is available to authorized users.

✉ Silvana Allodi
sallodi@biof.ufrj.br

Paula Grazielle Chaves da Silva
p.chaves@biof.ufrj.br

[1] Programa de Neurobiologia, Instituto de Biofísica Carlos Chagas Filho, Universidade Federal Do Rio de Janeiro, Ilha do Fundão, Rio de Janeiro, RJ 21949-902, Brazil

[2] Wellesley College, Wellesley, MA 02481, USA

Published online: 24 January 2020

TBI Traumatic brain injury
THCs Total hemocyte counts

Introduction

In the adult mammalian brain, it has been shown that immune cells support neurogenesis from neural progenitor cells (Smith et al. 2018; Ziv and Schwartz 2008). In decapod crustaceans, hemocytes (blood cells/immune cells) actively participate in neurogenesis, influencing the number of cells in the neurogenic niche (Benton et al. 2014). Additionally, hemocytes participate in neurodegeneration following injury (Benton et al. 2011; Chaves da Silva et al. 2010, 2013a); however, it is not known how this affects the neurogenic niche containing neural progenitors.

In the crayfish *Procambarus clarkii,* neural progenitors reside in a vascularized niche located on the ventral surface of the brain, just beneath the sheath. These niche cells are bipolar, with short processes that project to a vascular cavity located centrally in the niche, and long processes that extend to neuron clusters 9 and 10 (CL9, CL10) in the brain that contain local and projection neurons in the olfactory pathway. However, the niche cells do not undergo long-term self-renewal, instead having limited numbers of divisions to generate (transit-amplifying) daughters that proceed through several additional mitoses. Daughter clones migrate together along the processes of the bipolar niche cells to the brain cell clusters (Brenneis and Beltz, 2019; Sullivan et al. 2007a), where they differentiate into local and projection neurons (Fig. 1) (Sullivan and Beltz 2005).

In spite of the lack of long-term self-renewal, the neural progenitor cells are not depleted as crayfish grow and age, suggesting that this cannot be a closed system and that these must be replenished by a source external to the niche (Benton et al. 2013, 2014). In this context, in vitro experiments showed that hemocytes express a strong affinity for the niche (Benton et al. 2011). In addition, the number of cells composing the neurogenic niche in crayfish is positively correlated with total hemocyte counts (THCs) and can be manipulated by raising or lowering the number of circulating hemocytes (Benton et al. 2011). Finally, when labeled donor hemocytes are transferred to recipient crayfish, these can be found in the neurogenic niche as well as in CL9 and CL10, where they produce appropriate neurotransmitters (Benton et al. 2011; Brenneis and Beltz 2019). These findings suggest that hemocytes can enter the neurogenic niche and transform into neural progenitor cells. In insects, hemocytes have also been described as contributors to glial repair after selective disruption of glial cells in the abdominal nervous connectives, playing a critical role in both structural repair and recruitment of endogenous reactive cells (Howes et al. 1987; Smith et al. 1984, 1987). Together, these data provide evidence that hemocytes are a source of neural progenitor cells under physiological conditions and/or a potential tool to dedifferentiate into neural cells during lesion (Smith et al. 1987).

In the crayfish, hemocytes are produced in the hematopoietic tissue (HPT), which can be divided into three different regions: posterior HPT, anterior HPT, and the anterior proliferation center (APC) (Noonin et al. 2012). Data suggest that the APC contains multipotent stem cells and has direct access to regions where adult neurogenesis occurs (Chaves da Silva et al. 2013a; Noonin et al. 2012). Three types of hemocytes are produced by the HPT in crayfish (granular, semi-granular, and hyaline), and these have been studied due to their key roles in humoral and cell-mediated immune responses. Hemocyte activation initiates a series of events leading to phagocytosis, encapsulation, and secretion of enzymes that eliminate pathogens (Hillyer et al. 2010; Lin and Söderhäll 2011; Noonin et al. 2012; Novas et al. 2004). One of these enzymes is nitric oxide synthase (NOS), the enzyme that generates nitric oxide (NO) (Johansson and Carlberg 1994; Palumbo 2005; Tota and Wang 2005). NO production is among the early activation processes in pathogen defense, and this role has been conserved over the course of evolution (Palumbo 2005; Tota and Wang 2005). Under physiological conditions, NO is a messenger molecule that mediates diverse functions, such as blood vessel relaxation, immune activity, and neurotransmission in central and peripheral neurons. However, an excessive production of NO following a pathologic insult can lead to neurotoxicity (Beckman and Koppenol 1996; Lind et al. 2017).

Following traumatic lesion, NO can have both beneficial and detrimental effects (Beckman and Koppenol 1996; Lind et al. 2017). In the adult crab *Ucides cordatus*, inducible NOS (iNOS) is produced acutely by hemocytes containing granules (semi-granular and/or granular cells) as an immune response triggered by traumatic injury of the eyestalk, suggesting a signaling mechanism to attract other immune cell types that perform defensive roles (Chaves da Silva et al. 2010, b) such as phagocytosis of cell debris (Smith and Söderhäll 1983; Söderhäll et al. 1986).

In juvenile crayfish *P. clarkii,* an increase in NOS immunoreactivity was observed in the olfactory pathway 48 h after bilateral ablation of the antennule (Benton et al., 2007). The antennules contain olfactory receptor neurons projecting to the ipsilateral OL (Mellon and Munger 1990; Sandeman and Denburg 1976; Schmidt et al. 1992; Schmidt and Ache 1992, 1996a, b) and the lateral antennular neuropil (LAN) in the deutocerebrum (Harzsch and Krieger 2018; Sandeman and Denburg 1976; Schachtner et al. 2015; Tuchina et al. 2015; Yoshino et al. 1983). Once this olfactory pathway was damaged, NOS increase was associated with a reduction in neurogenesis in CL10

(Benton et al. 2007). Unilateral amputation of the crayfish (*Cherax destructor)* antennule also causes a reduction in the number of local interneurons and projection neurons on the ipsilateral side, which is associated with a decrease in the volumes of the olfactory and accessory lobes, to which these neurons project (Sandeman et al. 1998). Unilateral ablation of a crayfish antennule, therefore, effectively induces a neurodegenerative process.

In previous studies conducted in crayfish, we showed that the neurogenic niche is closely associated with the vasculature (Chaves da Silva et al. 2012; Sullivan et al. 2007b), as are niches in the mammalian brain (Doetsch et al. 1999; Pathania et al. 2010) where the immune and vascular systems are necessary for neuronal generation and neural stem cell fate determination (Leiter et al. 2016). In addition, the activation of the immune system may regulate adult neurogenesis by releasing inflammatory cytokines, whereas vasculature may contribute to the neural stem cell niche by providing a homing environment for neural stem cells (Horgusluoglu et al. 2017; Leiter et al. 2016; Smith et al. 2018).

The present study examines how the immune system responds to neural injury and the process of neurodegeneration, and the relationship of these events to neurogenesis in the crayfish *P. clarkii*. The olfactory lobe (OL) receives projections from the antennule and is targeted by the processes of CL9 and 10 neurons—the same cell clusters that contain adult-born neurons. A previous study in the crayfish *C. destructor* showed that antennular ablation resulted in both neurodegeneration and a later increase in bromodeoxyuridine (BrdU)-labeled profiles in CL10 during the period when the antennule was being reconstituted (Sandeman et al. 1998). This suggested that antennular ablation may influence both neurodegeneration and neurogenesis. Thus, the present study investigates the acute and short-term effects of unilateral antennular ablation on the neurogenic niche, focusing particularly on the role of hemocytes and the response of the vasculature.

Materials and Methods

Animals

Adult male and female freshwater crayfish *P. clarkii* (Malacostraca, Decapoda, Astacidae; carapace length 15–20 mm) were obtained from Carolina Biological Supply Company (Burlington, NC) and maintained at 21 °C in aquaria with artificial pond water and a 12:12-h light:dark cycle. Maintenance of crayfish was overseen by full-time staff in the AALAC-approved Animal Care Facility at Wellesley College. All procedures were conducted according to animal welfare guidelines.

Antennular Ablation and BrdU Assays

Crayfish antennules are frequently damaged during aggressive displays, and the surgical approach used was intended to mimic commonly occurring damage. The antennular flagella of juvenile crayfish ($n=5$ crayfish per group) were ablated unilaterally just proximal to the bifurcation point (Fig. 1e), in order to cause a traumatic injury. All injuries were performed on the right side; "ipsilateral" is used throughout to refer to the same side as the injury. Brains were dissected and assayed immunohistochemically for iNOS, universal NOS (uNOS), and glutamine synthetase (GS) at several time points after unilateral ablation (15 min, 1 h, 24 h, 48 h, 5 days). Proliferation of cells in CL9 and CL10 and the neurogenic niche were examined at 24 h, 48 h, and 5 days after ablation (Fig. 1e-black line); crayfish were incubated in the S-phase marker BrdU (Sigma-Aldrich, St. Louis, MO) (2 mg/mL artificial pond water) for 24 h before sacrifice (Fig. 1e-green line). Unablated animals of the same size were used as controls ($n=5$). Standard immunohistochemical methods were used for the detection of BrdU (see 2.4 below).

Total Hemocyte Count (THC) Following Antennular Ablation

Hemolymph was collected from 5 crayfish just prior to antennular ablation and at 24 h, 48 h, and 5 days following ablation. A 25-gauge 5/8″-long ice-cold needle was used to obtain a hemolymph sample. The needle was inserted superficially just ventral to the abdominal musculature, to the left or right of the abdominal artery. The needle was gently removed when approximately 30–40 µL of blood was collected in the hub of the needle.

For each sample, 10 µL of hemolymph was pipetted immediately into an Eppendorf tube on ice containing 20 µL of anticoagulant buffer (0.14 M NaCl, 10 mM EDTA, 30 mM trisodium citrate, 26 mM citric acid, 0.1 M glucose; pH 4.6) in order to prevent blood clotting. The buffer and plasma solution was then mixed 1:1 (vol:vol) with trypan blue in order to label cells. Trypan blue is an azo dye that selectively stains dead cells, and was used here so that these could be distinguished from live cells during the counting procedure. The resulting solution was pipetted into a disposable 4-chip hemocytometer (Bulldog Bio, Inc., Portsmouth, NH) and the number of cells counted using standard methods. Calculations were done to account for the dilution of the sample and to represent counts as the number of cells per milliliter of hemolymph (the THC). THC after antennular ablation was normalized by calculating the percent change from pre-ablation THC levels and by presenting these as

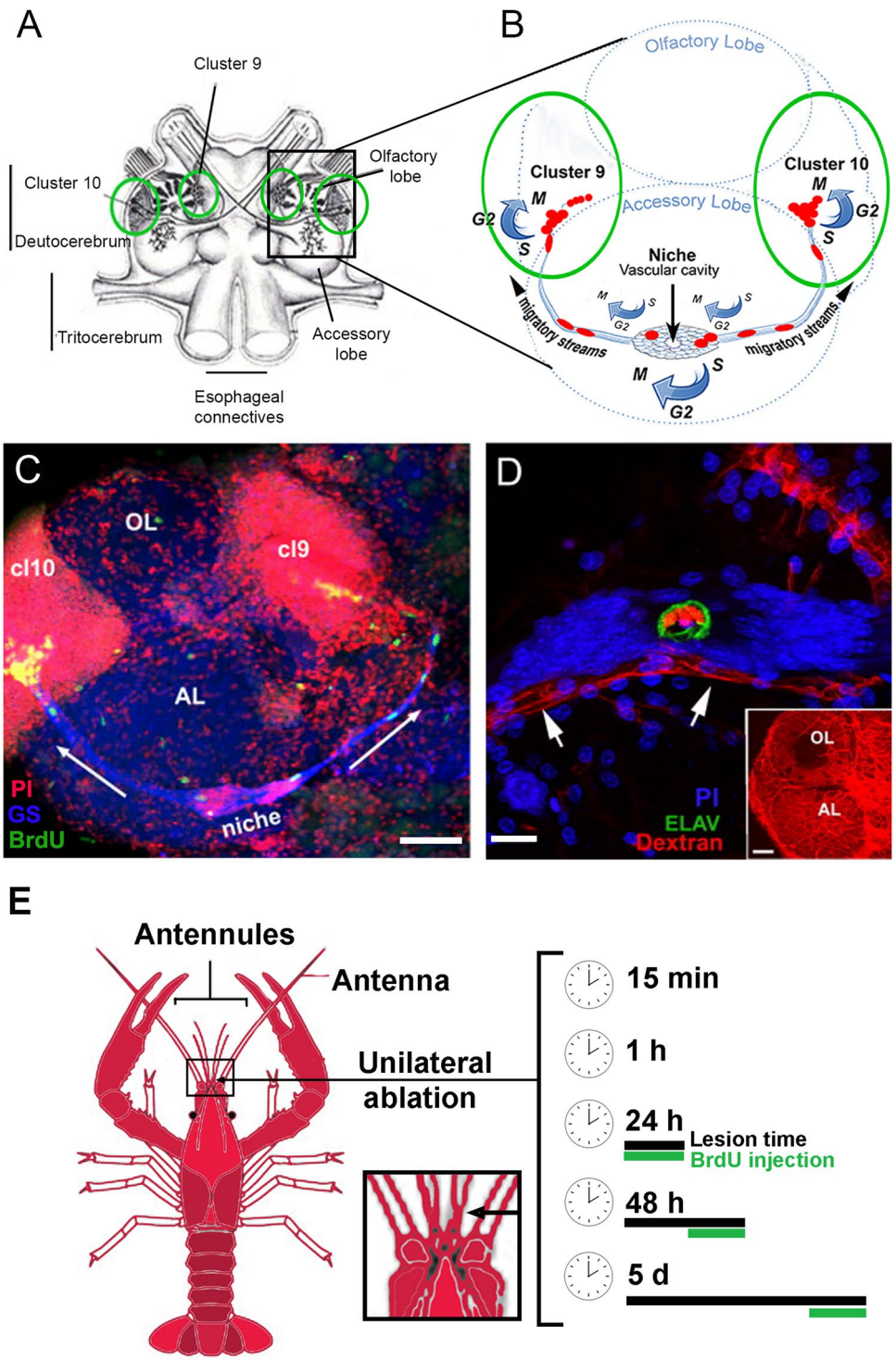

relative THC values. Results are expressed as mean ± SE (24 h: 1.50 ± 0.49; 48 h: 1.20 ± 0.36; 5 days: 0.98 ± 0.06).

Immunohistochemical Protocols

Dissected brains ($n = 5$ per group) were immersion fixed with 4% paraformaldehyde in 0.1 M phosphate buffer (PB; 20 mM NaH_2PO_4, 80 mM Na2HPO4; pH 7.4) for 12–24 h and then rinsed in PB. Standard immunohistochemical methods were used to localize specific antigens. Primary antibodies diluted in PB with 0.3% v/v Triton X-100 (PBTx) were applied to tissues overnight at 4 °C. The following primary antibodies were used to label cells in the neurogenic niche and the surrounding region: mouse anti-GS (1:100; Becton

◂**Fig. 1** Adult neurogenesis in the crayfish (*Procambarus clarkii)* brain**. a** The neurogenic system in the adult brain is located in the deutocerebrum, which contains the olfactory (OL) and accessory (AL) lobes. The diagram of the brain shows clusters 9 (CL9) and 10 (CL10) (green circles), respectively, where later divisions of progenitor cells occur. **b** Region indicated in the black square in A, showing the OL and AL and the neurogenic niche containing the 1st generation neural progenitors. Following several divisions in the niche, migratory streams, and proliferation zones, daughter cells integrate into CL9 and CL10, where they differentiate. **c** Immunofluorescence showing the niche and the migratory streams on the surface of the AL labeled immunocytochemically for glutamine synthetase (GS, blue). BrdU+cells (green) were observed in the niche, migratory streams, and in the cell clusters. Propidium iodide (PI, red) labels cell nuclei. **d** The neurogenic niche is closely associated with the vasculature. This is shown by injecting dextran dye (red) into the cerebral artery in order to fill the blood vessels in the brain. The dextran is observed in a blood vessel just beneath the niche and in the vascular cavity, which is delineated by ELAV immunoreactivity (green), suggesting a direct vascular connection to the niche. **e** Diagram of the crayfish *P. clarki* showing the antennules and the ablation point (arrow). The inset shows a higher magnification of the cut region—right below the bifurcation. The time points used to analyze the samples after ablation (15 min, 1 h, 24 h, 48 h, 5 days) are shown on the right side as well as the BrdU injections performed 24 h before sacrifice (green line)—only 24 h, 48 h, and 5 days after ablation. PI (blue). Scale bars: **c** 100 µm; **d** 20 µm. (Images **a** and **b** adapted from Beltz and Benton 2017; **c** and **d** from Sullivan et al. 2007b)

Dickinson, Franklin Lakes, NJ) or mouse anti-tyrosinated tubulin (1:1000; Sigma-Aldrich, Saint Louis, MO); rat anti-BrdU (1:50; Accurate Chemical, Westbury, NY); rabbit anti-uNOS (1:200; Affinity BioReagents, Golden, CO); and rabbit anti-iNOS (1:100; Sigma-Aldrich, Saint Louis, MO). After primary antibody incubations and rinses in PBTx, tissues were incubated in the complementary secondary antibodies overnight at 4 °C: goat anti-rat Alexa 488; goat anti-mouse Alexa 649; and goat anti-rabbit Alexa 488 (1:100; all from Jackson ImmunoResearch Laboratories, Inc., West Grove, PA). After several rinses in PB, brains were stained with the nucleic acid marker propidium iodide (PI; 1:100, Sigma-Aldrich, Saint Louis, MO), which facilitated counting the total number of niche cells. Brains were then mounted using Fluoro-Gel (Electron Microscopy Sciences, Hatfield, PA) and viewed with a confocal microscope. Some images were adjusted for brightness and contrast with Adobe Photoshop 6.0 software (Adobe Systems, CA, USA). Secondary antibody specificities were tested by omitting the primary antibodies.

Dextran Injections

Fluorescein isothiocyanate (FITC)-conjugated dextran 3000 MW (Invitrogen, Carlsbad, CA) (400 µL of a 1 mM solution in crayfish saline: 205 mM NaCl, 5.4 mM KCl, 34.4 mM CaCl2, 1.2 mM MgCl2, and 2.4 mM NaHCO3) was injected into the pericardial sinus of crayfish in order to label the brain vasculature, including that associated with the neurogenic niche. Animals (15–20 mm carapace length; $n=5$ per group) were placed in artificial pond water for 30 min following injection. The brains were dissected in saline and the sheath was preserved in order to maintain the vasculature surrounding the niche. The brain was then fixed in 4% paraformaldehyde overnight at 4 °C. Using standard immunohistochemical techniques, tissues were labeled with mouse anti-GS (1:100; Becton Dickinson, Franklin Lakes, NJ) followed by overnight incubation in goat anti-mouse Alexa 649 (1:100; Jackson ImmunoResearch, West Grove, PA) and then stained with the nuclear marker PI.

Electron Microscopy

Dissections of unablated (control) brains ($n=5$) were performed in cold crayfish saline. The fixation was done by immersion in 4% paraformaldehyde, 2.5% glutaraldehyde, and 0.5% tannic acid in PB (pH 7.2) for 2 h. Samples were then post-fixed in 1% osmium tetroxide in PB in the dark for 30 min. Samples were rinsed in PB and stained *en bloc* in 1% uranyl acetate overnight, dehydrated in a graded ethanol series up to 100%, and embedded in Spurr Resin (Electron Microscopy Sciences, Kit #14,300). Following polymerization for 12 h at 80 °C, semi-thin sections (400–500 nm) were obtained with a Sorvall MT-5000 ultramicrotome (DuPont de Nemours, Wilmington, DE), stained with a mixture of toluidine blue and borax, and examined with a light and fluorescent compound microscope (Zeiss Axioskop 2 microscope equipped with a CCD color camera Evolution™MP; Media Cybernetics, Rockville, MD). Ultrathin sections (60–70 nm) were then obtained from blocks of interest using a RMC MT 6000 ultramicrotome, stained with uranyl acetate and lead citrate, and examined with a JEOL 1200 EX transmission electron microscope operated at an accelerating voltage of 80 kV.

Data Analysis and Statistics

Cell Counting

The number of PI+cells in the niche and BrdU+cells in CL9 and CL10, the niche, and its vicinity were counted from 3D stacks of optical images. A single optical section was projected onto the monitor and the labeled cells traced onto a transparent sheet. This was repeated for each section and the cells were then counted from the transparencies. In order to quantify BrdU+cells in the vicinity of the niche, a circular zone (500 µm diameter) around the niche was delimited; the vascular cavity in the niche was considered the center of the zone. Only BrdU+cells within the selected area were counted (circled in Fig. 3). iNOS− and GS+cells (Figs. 5 and 8) around the neurogenic niche were also counted. In this case, fluorescence confocal images

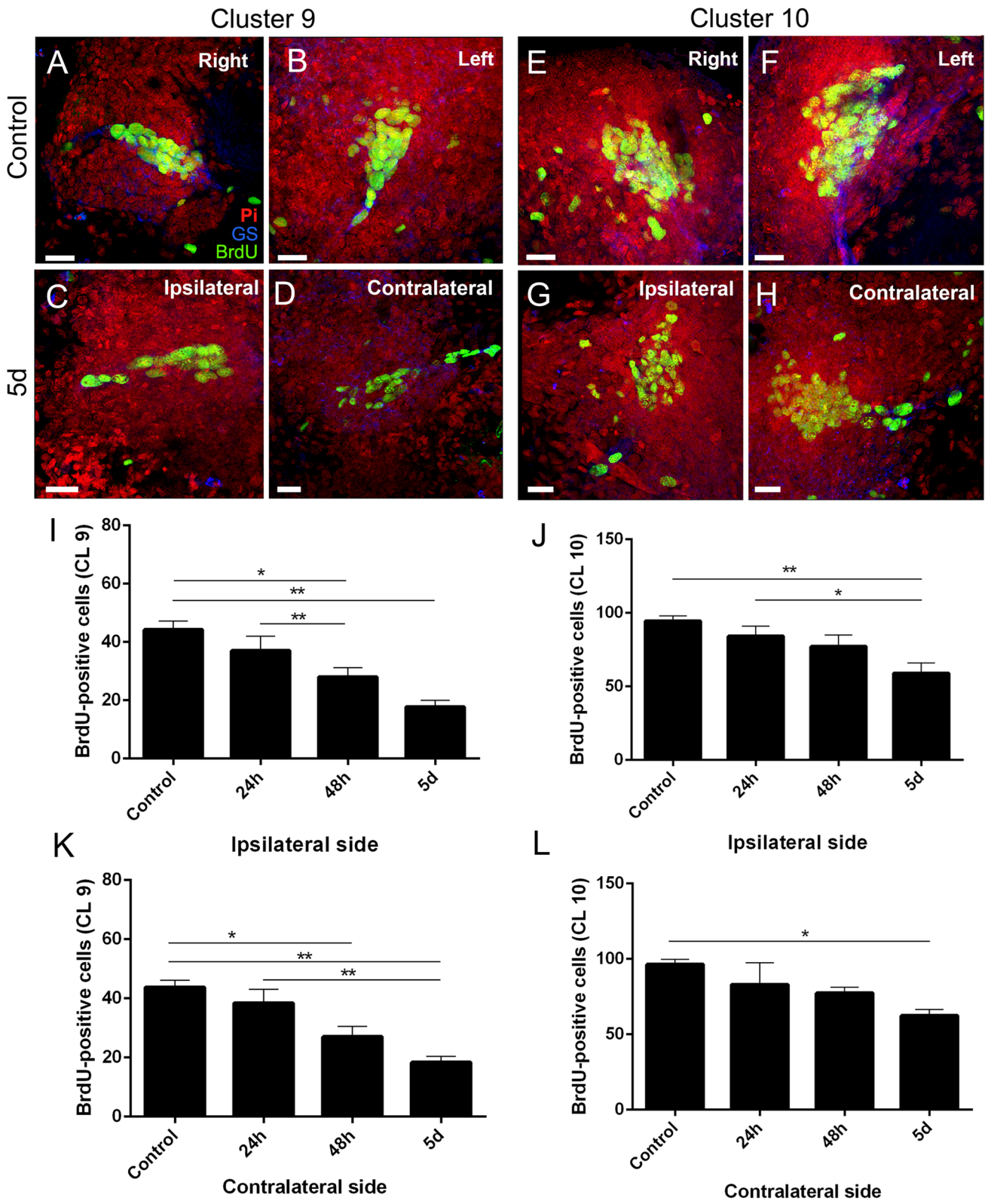

at the same magnification were used to count all labeled cells in the entire microscopic field, positioning the vascular cavity in the center of the images. All data are shown as mean ± SEM. Comparisons between different groups of animals were made by using ANOVA with the Tukey post hoc test (for total niche cell counting) and Kruskal–Wallis

◂**Fig. 2** The number of BrdU+cells in CL9 and CL10 decreases bilaterally following antennular ablation. **a**–**h** BrdU+(green) cells in CL 9 and 10 in controls **a**, **b**, **e**, **f** and 5 days after ablation **c**, **d**, **g**, **h**, **i**, **j** Number of BrdU+cells in the clusters after ablation (24 h, 48 h, and 5 days) on the ipsilateral and contralateral side **k**, **l**. The number of BrdU+cells decreased in the ipsilateral CL9 **i** and CL10 **j** compared with the control groups. Note that the ipsilateral CL10 did not exhibit any change in the number of cells until 5 days after ablation. * $p < 0{,}05$. ** $p < 0{,}005$. ($n = 5$). PI (red) labeled cell nuclei. Glutamine synthetase (GS, blue) labels the migratory streams as these enter CL9 and CL10 (most visible in **f**). Scale bars: **a**-**h** 30 µm

with Newman–Keuls post hoc test (for BrdU and iNOS labeled cells). A value of $p < 0.05$ was considered statistically significant.

Analyses of Blood Vessel Changes

The density of dextran-FITC labeling (Fig. 11) was measured using the program Image J and the percentage of dextran fluorescence was then quantified. The same parameters (such as magnification, fluorescence intensity, and binary image conversion) were adjusted equally for all images in each group, including controls. The blood vessels were counted from the ventral to the dorsal surface of the niche in brains with intact sheaths (throughout the Z-stack confocal image). In order to measure the caliber of the blood vessels surrounding niches on both sides of the brain, the average of the five largest vessels revealed by the FITC fluorescence in each image was calculated. All data are shown as mean ± SEM. Comparisons between different groups of animals were made with Kruskal–Wallis nonparametric test, followed by Neuman–Keuls post hoc analysis, using Prism software (GraphPad Software, San Diego, CA).

Results

Four types of cell counts were used to assess the effects of antennular ablation on the immune response and adult neurogenesis: (1) The number of BrdU+cells was quantified in the neurogenic niche, CL9 and CL10, in order to analyze the effect of the ablation on neural proliferation. BrdU+cells in the vicinity of the niche were also examined because this region has a close physical relationship with the niche and neural progenitor cells are likely to access the niche by passing through this area; (2) PI-labeled cells in the niche were counted to determine the total number of niche cells; (3) The number of iNOS+cells in the area around the niche was quantified as one measure of the immune response after ablation; (4) The THC was calculated at various time points after antennular ablation, as a second measure of the immune response.

Proliferative Cells in the Niche and Brain Clusters 9 and 10 Decrease Bilaterally After Unilateral Antennular Ablation

The crayfish antennule is a structure containing olfactory receptor neurons that project to the ipsilateral OL (Mellon and Munger 1990; Sandeman and Denburg 1976; Schmidt et al. 1992; Schmidt and Ache 1992, 1996a, b), as well as mechanoreceptors, statocysts, and nonaesthetasc chemoreceptors that project to the ipsilateral lateral antennular neuropil (LAN) in the deutocerebrum (Harzsch and Krieger 2018; Sandeman and Denburg 1976; Schachtner et al. 2005; Tuchina et al. 2015; Yoshino et al. 1983). These pathways were examined in the present study.

Cutting the antennular nerve triggers an initial response characterized by a reduced volume of the ipsilateral OL due to the death of olfactory afferents (Sandeman et al. 1998). In the present study, in order to observe the effect of antennular ablation on a population of newborn neurons that project to the OL, we quantified BrdU+local and projection neurons in CL9 and CL10, respectively, at 24 h, 48 h, and 5 days after unilateral ablation (Fig. 2) Following unilateral ablation, the number of BrdU+cells decreased bilaterally in both cell clusters (CL9 and CL10) compared with the control group (Fig. 2i-l). However, CL9 showed an earlier response (48 h after ablation) than CL10 (Fig. 2i, k). Neither ipsilateral nor contralateral CL10 exhibited statistically significant changes in the number of BrdU+cells until 5 days after ablation (Fig. 2j, l). The neurogenic niche contains neural progenitor cells, and at any given time 2–4 cells can usually be labeled with BrdU, indicating that they are actively in the cell cycle. Mitotic divisions of cells next to the vascular cavity and of cells within the niche have also been observed (Brenneis and Beltz, 2019). Their migrating progeny travel along the processes of the niche cells to the proliferation zones associated with CL9 and CL10, where the adult-born neurons divide again and differentiate. These cells require 5–7 days to migrate from the niche to CL9 and CL10, where they undergo neural differentiation (Sullivan et al. 2007a; Benton et al. 2011; Sullivan and Beltz 2005). Since both neuron clusters had fewer proliferating (BrdU+) cells after antennular ablation (Fig. 2), BrdU+cells in the neurogenic niche were also counted to evaluate whether the ablation also caused a change in the number of proliferating neural precursor cells (Fig. 3). In addition, BrdU+cells were often observed embedded in the connective tissue or blood vessels surrounding the niche, and these were also quantified (Fig. 3f, h). Twenty-four hours after the ablation (see Fig. 1e), the number of BrdU+cells in the niche did not differ significantly from that in the control; however, there were fewer BrdU+cells surrounding the niche, in the connective tissue or within the blood vessels near the niche. Forty-eight hours after the ablation the number of BrdU+cells was

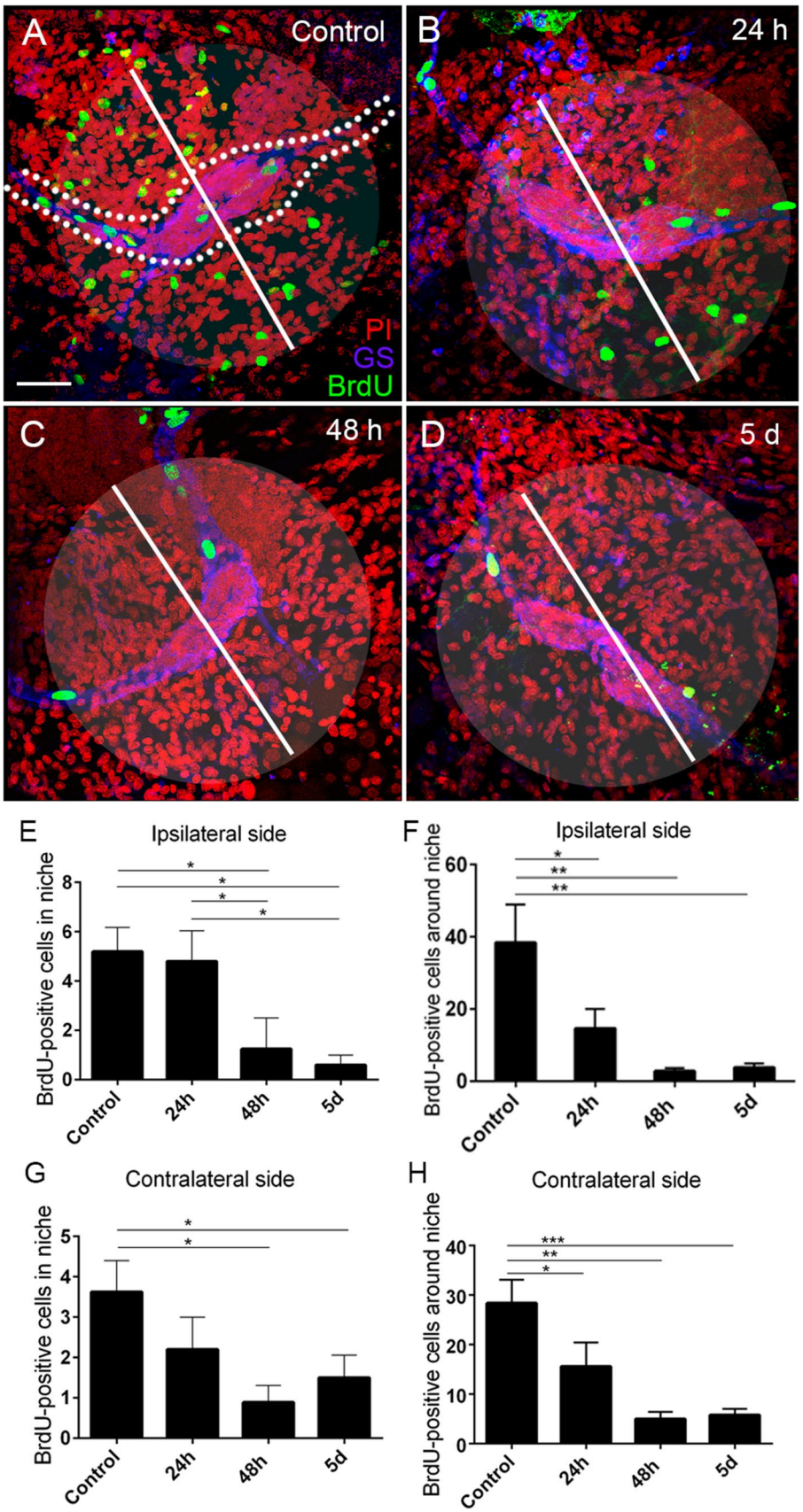

Fig. 3 The number of BrdU+cells in the neurogenic niche and surrounding region decreases bilaterally after ablation. **a** Control. The neurogenic niche is outlined. **b** 24 h after ablation, the number of BrdU+cells (green) in the niche ipsilateral to the ablation remained similar to the control, however, there were fewer cells in a measured area surrounding the ipsilateral niche (circular area indicated in **a–d).** The white line represents the diameter of the circular counting area, with the center of the line positioned on the vascular cavity in the niche. **c** By 48 h after ablation, the number of BrdU+cells was sharply reduced both within and surrounding the ipsilateral niche, remaining lower for at least 5 days post ablation (**d**). Quantitative analyses of the number of BrdU+cells within **e**, **g** and surrounding **f, h** the niche in the control and lesioned animals (24 h, 48 h, and 5 days). * $p<0{,}05$. ** $p<0{,}005$. ($n=5$). GS (blue) labels the niche and streams; PI (red) labels cell nuclei. Scale bars: **a**–**d** 100 µm

significantly lower both within and surrounding the niche, and remained reduced for at least 5 days post ablation. This response was observed bilaterally (Fig. 3g, h).

We therefore asked whether the total number of niche cells was altered by antennular ablation. On the side ipsilateral to the lesion, niche cell numbers did not differ significantly from control (Fig. 4a). On the contralateral side, a small increase (10–15%) in niche cell numbers was observed that was statistically significant only at 48 h after the ablation, with numbers returning to control values by 5 days (Fig. 4b). However, an analysis of both ipsilateral and contralateral niche cell numbers demonstrated no statistical difference between these (Fig. 4c).

These results show that unilateral antennular ablation suppresses neural progenitor cell proliferation bilaterally in the neurogenic niche and brain cell clusters during the first 5 days following ablation (Figs. 2 and 3), while the total number of niche cells is relatively stable (Fig. 4).

Antennular Ablation Increases iNOS Labeling in the Vicinity of the Neurogenic Niche

According to an earlier study in which the antennule was ablated in juvenile lobsters (*Homarus americanus*) (Benton et al. 2007), increased NOS immunoreactivity was observed in the brain in the first 2 days following ablation; this study used a universal NOS (uNOS) antibody that recognizes all three isoforms of NOS. However, the neurogenic niche was not the focus of this previous study. In the current study, we therefore conducted experiments that aimed to identify a specific NOS isoform, inducible NOS (iNOS), which is mainly expressed in macrophages, astrocytes, and microglial cells upon neurotoxic, traumatic, and inflammatory damage (Calabrese et al. 2007). Below, we show the results related to the immune response (iNOS labeling) after unilateral ablation.

iNOS labeling was observed bilaterally in the area immediately adjacent to the niche at 1 h, 24 h, 48 h, and 5 days after ablation (Fig. 5). Unablated (control) animals did not show iNOS labeling around the niche (Fig. 5a, f). One hour after ablation, the ipsilateral side showed an increase of iNOS+ cells around the niche and within the vascular cavity (Fig. 5b, k), whereas the contralateral side showed weak labeling around the niche and punctate labeling in the vascular cavity (Fig. 5g, l) compared with the control (Fig. 5a, f). We also observed GS+ cells near the ipsilateral niche, but iNOS labeling did not colocalize in these cells (see text below and Fig. 8). Twenty-four and forty-eight hours after ablation, the vascular cavity and a wide area around each niche was labeled bilaterally by anti-iNOS, (Fig. 5c, d, h, i). The iNOS immunoreactivity was clearly less extensive on the contralateral than ipsilateral side 5 days after ablation, suggesting that this begins to subside first on the side further from the ablation (Fig. 5e, j). The number of iNOS+ cells in the vicinity of the ipsilateral niche was higher than the control throughout the experimental period, never re-establishing the control number of labeled cells (Fig. 6a), while the number of iNOS+ cells near the contralateral niche increased by 24 h after ablation and control levels were re-established by 5 days (Fig. 6b). Additional data are provided in Online Resource 1.

Because the number of iNOS+ cells in the vicinity of the niche increased bilaterally 24 h after ablation, we reasoned that this might be one element in the immune response to ablation. We then counted the total number of cells circulating in the hemolymph, THC, following antennular ablation (see Sect. 2.3), since a change in THC would also be an expected part of any immune system response. We observed that relative THC values (compared with pre-ablation

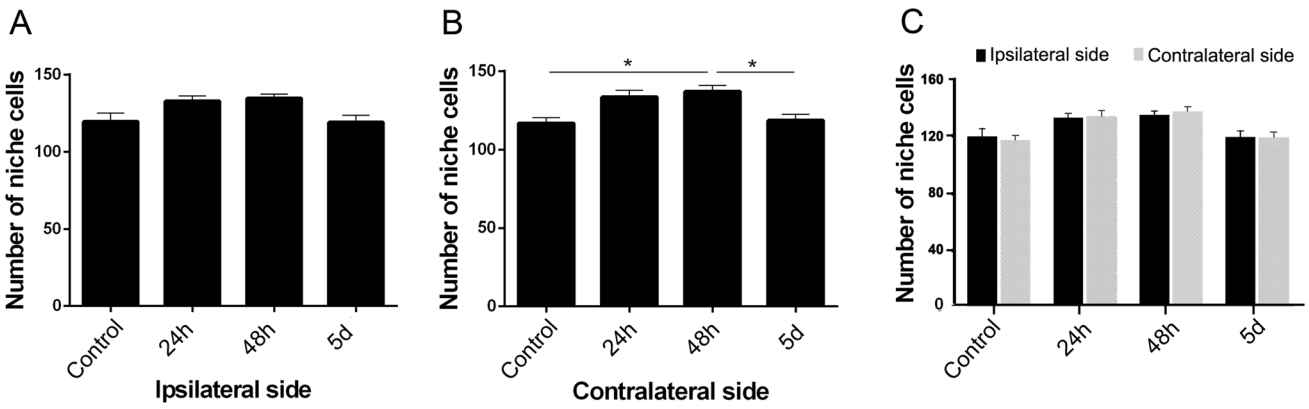

Fig. 4 Unilateral ablation does not alter the total number of niche cells. **a** Number of niche cells in the ipsilateral niche (24 h, 48 h, and 5 days) after ablation. There was no significant difference among the time points. **b** Number of niche cells in the contralateral niche (24 h, 48 h, and 5 days) after ablation. *$p < 0{,}05$. **c** Number of niche cells on both sides were compared at each time point. No significant difference was observed in the number of niche cells on the ipsilateral and contralateral sides

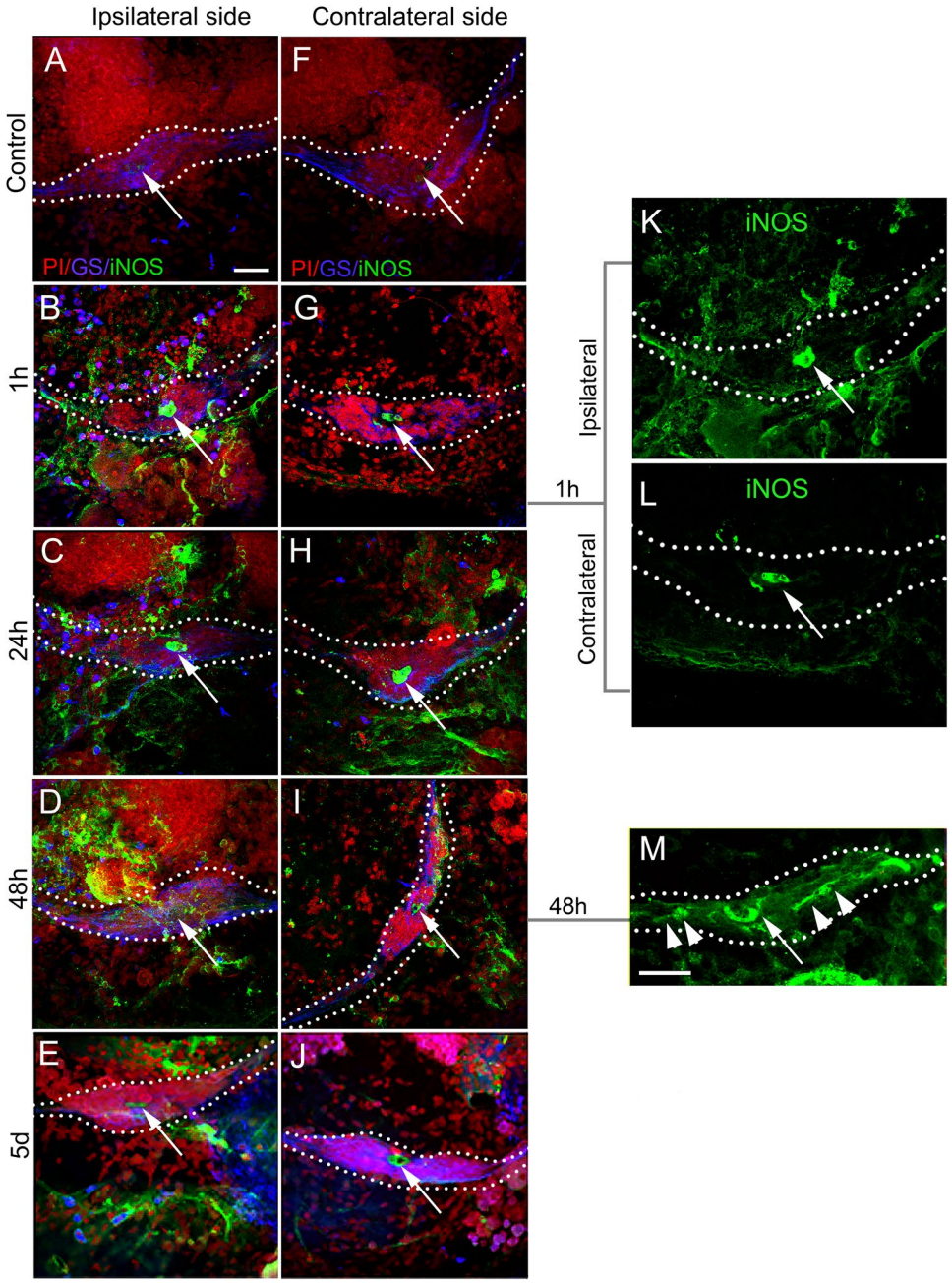

Fig. 5 Antennular ablation increases the number of iNOS+ cells adjacent to the neurogenic niche. **a–e** Ipsilateral side. **f-j** Contralateral side. **a**, **f** Controls. **b** 1 h after ablation iNOS+ cells (green) around the niche and within the vascular cavity (arrow; arrows in **a**–**l** indicate the vascular cavity) were observed on the side ipsilateral to antennular ablation. The contralateral side **g** showed weak labeling around the niche and more intense labeling in the vascular cavity compared with the control. **c, h** 24 h after ablation the vascular cavity (arrow) and a wide area around the niche were labeled bilaterally with anti-iNOS. **d**, **i** 48 h after ablation some niche cells (arrowheads in M) as well as the area around the niche on both sides of the brain were labeled by anti-iNOS. iNOS labeling was less extensive in the contralateral side 5 days after ablation **j** than 48 h after ablation (**i**). **k**, **l** The same region of **b** and **g**, respectively, showing higher magnification images of iNOS labeling. **m** Ipsilateral niche 48 h after ablation (different image than in **d** and showing only the iNOS channel). GS (blue) labels cells in the niche and their processes in the migratory streams. We can also see GS+/iNOS− cells, possibly hemocytes, around the niche; PI (red) labeled cell nuclei. Scale bars: 50 µm

controls) also increased by 24 h after the lesion, gradually returning to control values by 5 days (Fig. 6c). However, in the present study, we did not assess whether iNOS+ cells are responsible for the increase in THC.

The iNOS labeling also extended to the OL and to cluster 16 (CL16) (Fig. 7), which contains the cell bodies of neurons that project to the OL and LAN. CL9 and CL10 did not show intense iNOS labeling but appear to contain scattered individual iNOS+ cells. Fifteen minutes after ablation, iNOS+ cells were observed connecting CL16, which was not previously known to be involved in neurogenesis, to the ipsilateral neurogenic niche (Fig. 7c; see also control in Fig. 7b). One hour after ablation, iNOS+ cells were found in groups or scattered near the niche (Fig. 7e). iNOS+ cells were also noted in the niche 1 h after ablation (Fig. 7f, asterisk). Figure 7f also shows cells near the niche that are GS+ but iNOS−, indicating that there are at least two populations of cells around the niche within the first hour after antennular ablation: GS+/iNOS− and iNOS+. Because GS+ cells around the niche did not colocalize with BrdU labeling (Fig. 3b), we hypothesize that these cells reach the niche from an external source instead of proliferating in the region around the niche.

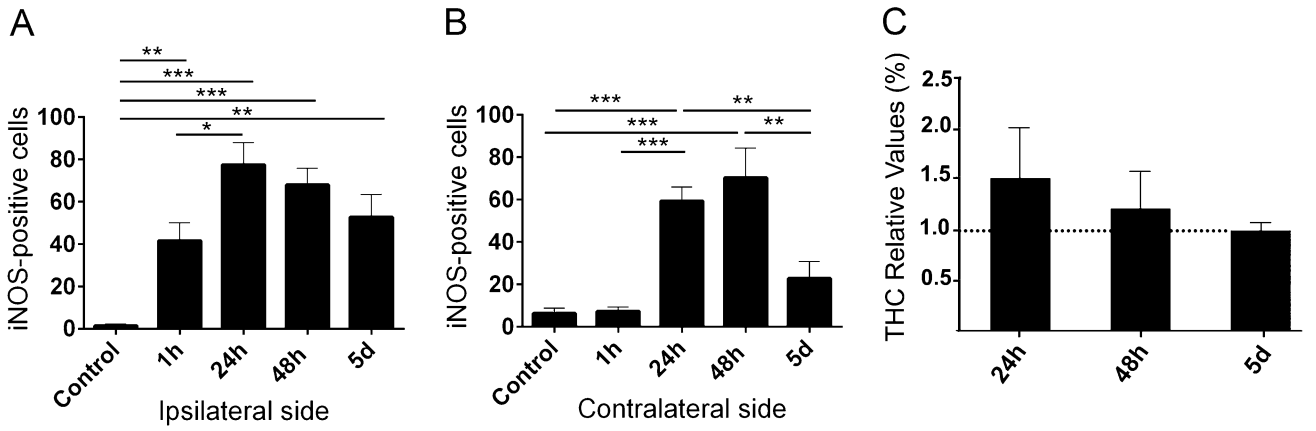

Fig. 6 The number of iNOS+ cells around the niche and total hemocyte counts (THC) increase after ablation. **a,b** Quantification of iNOS+ cells in the vicinity of the niche on the ipsilateral **a** and contralateral **b** sides ($n=5$). See Sect. 2.7 for counting method. (*$p<0.05$. ** $p<0.005$.) **c** Average relative THCs were calculated for each time point (24 h, 48 h, and 5 days). 24 h: mean: 1.50; SE: 0.49; 48 h: mean: 1.20; SE: 0.36; 5d-mean: 0.98; SE: 0.06). See Sect. 2.3 for counting method

GS immunolabeling has been used to identify niche cells in *P. clarkii* (Sullivan et al. 2007b; Zhang et al. 2009). As expected, anti-GS antibodies labeled niche cells in the current studies. In addition, anti-GS also labeled granular and semi-granular hemocytes near the niche, which were evident 1 h and 24 h after ablation near the ipsilateral niche (Fig. 8c, e); this number decreased to control levels by 48 h post ablation, which was maintained at the 5 days time point (Fig. 8g). However, the contralateral side did not show statistical difference in the number of GS+ cells in the vicinity of the niche at any of the time points after ablation (Fig. 8d, f).

These results suggest that the immune response triggered by antennular ablation is somewhat lateralized, with more dramatic changes ipsilateral to antennular damage, especially in the first few hours after lesion. This is unlike the findings related to neurogenesis reported above, in which there was a bilateral suppression of cell proliferation in the niche and brain cell clusters following unilateral antennular ablation.

uNOS/GS-Labeled Cells are Associated with the Lateral Antennular Neuropil After Antennular Ablation

Because mechanoreceptors, statocysts, and nonaesthetasc chemoreceptors from the antennule project to the ipsilateral LAN in the deutocerebrum (Sandeman and Denburg 1976; Schmidt et al. 1992; Schmidt and Ache 1996b; Tuchina et al. 2015; Yoshino et al. 1983), we asked whether the ablation of the ipsilateral antennule would affect the LAN. Also, we used a uNOS antibody that recognizes all three isoforms of NOS in order to observe whether these cells would be labeled similarly to iNOS. Interestingly, antennule ablation did not alter the gross morphological appearance of the LAN, however, 15 min after ablation uNOS + (Fig. 9b, ci) cells were observed in this region. Because the LAN is a synaptic region that does not contain neuronal cell bodies and because of the rapidity of their appearance after ablation, it is assumed that the uNOS + cells are associated with the vascular/immune system. Further, we observed cells labeled with GS, uNOS, and PI within blood vessels dorsal to the niche, also suggesting that these cells reach the LAN via the circulation (Fig. 9e). One hour after ablation, we observed uNOS + labeling colocalized with GS in semi-granular and/or granular hemocytes around the LAN, which is directly associated with the antennules, but (to our knowledge) not with the neurogenic niche. In this case, however, the two labels are not in the same cellular domains (Fig. 9d). Triple-labeled (GS, uNOS, and PI) cells near the niche were also observed (Fig. 9f).

Effect of Antennular Ablation on the Vasculature Dorsal to the Niche

A notable feature of the neurogenic niche in the crayfish brain is its close relationship with blood vessels, which are embedded in the surrounding connective tissue. Evidence supports the view that blood vessels, perivascular cells, and hemocytes penetrate the connective tissue upon which the niche rests (Chaves da Silva et al. 2012). Electron micrographs of cells within the blood vessels located dorsal to niche in control crayfish show that these cells can cross the vessel lining (Fig. 10) and pass through the connective tissue (Fig. 10d, e), potentially gaining access to the niche.

Because we observed a close spatial relationship between the neurogenic niche and the vasculature (Chaves da Silva et al. 2012; Sullivan et al. 2007b), we wanted to visualize the blood vessel network and how

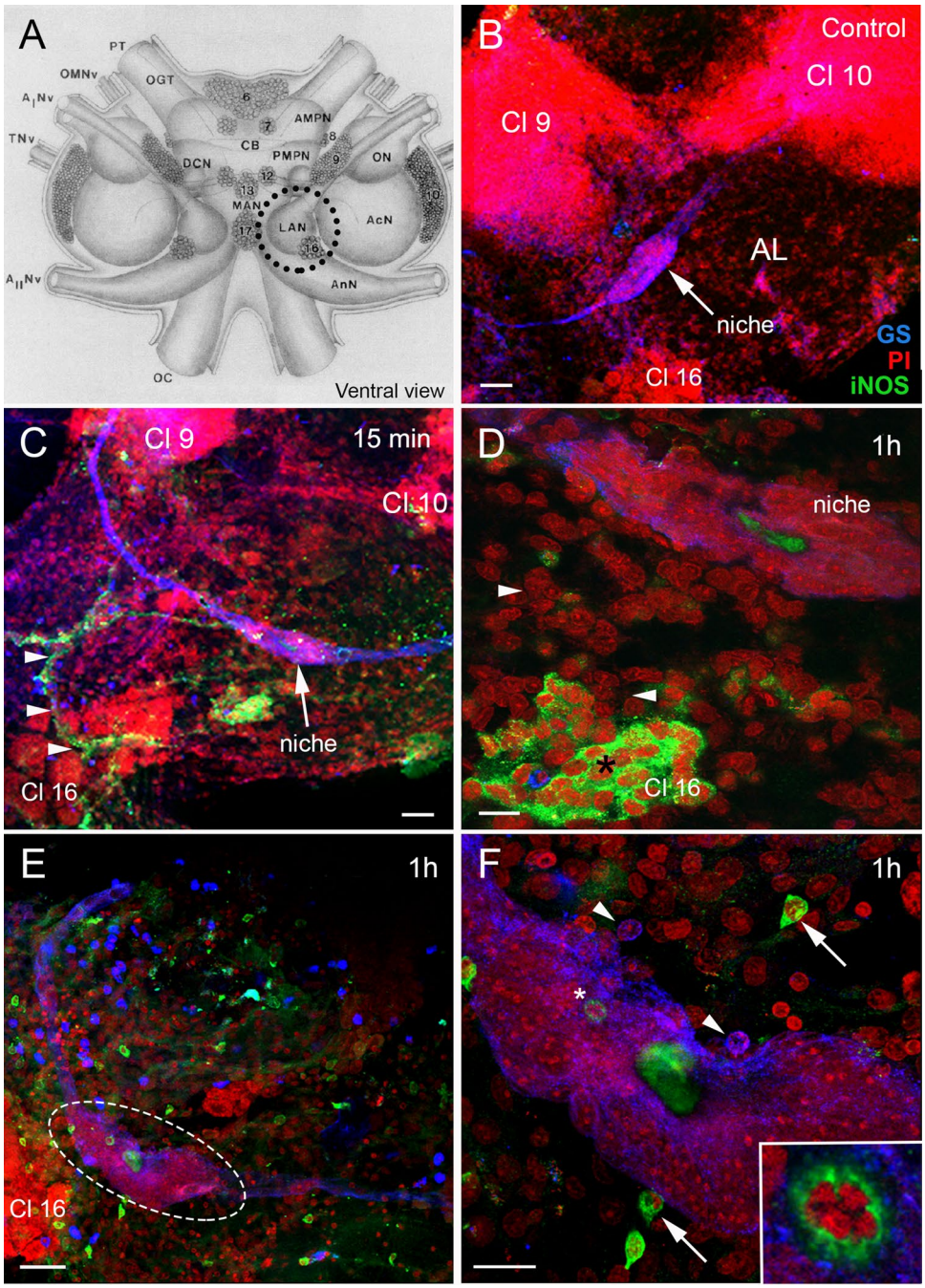

Fig. 7 iNOS+ cells are found in CL16 after antennular ablation. **a** Schematic diagram of the crayfish brain showing the LAN and cluster 16 (CL16) (black circle). **b** Control brain (unablated) showing the niche (arrow) labeled with GS (blue) on the surface of the accessory lobe (AL). Cells in the neuron clusters (CL 9, 10, and 16) are labeled with the nucleic acid marker PI (red). **c** 15 min after ablation iNOS+ cells (green) were observed (arrowheads) between CL16 and the ipsilateral neurogenic niche. **d** iNOS+ cells were observed in groups near the niche 1 h after lesion. **e** Both iNOS+(green) and GS+(blue) cells were observed near the niche (white circle) 1 h after lesion. Note that iNOS and GS labeling did not colocalize to the same cells. **f** iNOS+ cells (arrows) near or within the niche (asterisk) 1 h after ablation. Insert shows a high magnification of the iNOS+cell within the niche and its nucleus (PI: red). Note that some GS+cells (arrowheads) are also located near the niche. Scale bars: **b**, **c** 100 µm; **d** 30 µm; **e** 60 µm; **f** 15 µm. (Image **a** originally from Sandeman et al. 1992, Figure 3B on page 309. Order license # 4653110596087 obtained on 08/20/2019)

it is affected by antennular ablation. Dextran-FITC was injected into the dorsal artery of both control and ablated animals during the peak iNOS labeling period (1 h, 24 h, and 48 h after ablation). Crayfish were killed 30 min after dextran injection, and the brains were processed for immunohistochemistry using GS antibody to identify niche cells (Fig. 11). In controls, as expected, dextran labeling showed a complex blood vessel network surrounding the niche (Fig. 11a, ai). However, by one hour after antennular ablation the ipsilateral niche was completely surrounded by a much denser system of blood vessels filled with dextran (Fig. 11b, e), suggesting that neovascularization or dilation of small vessels is occurring in response to the ablation. On both ipsilateral and contralateral sides, the region covered by blood vessels increased in the 24 h following ablation (Fig. 11b, c, e, f). The density of the vascular network on both sides returned to control levels by 48 h after ablation (Fig. 11d–f). In order to identify whether the increase in the dextran-labeled region was related to blood vessel caliber after ablation, we measured the diameter of blood vessels (FITC fluorescence) surrounding the neurogenic niche in all experimental conditions. The results show

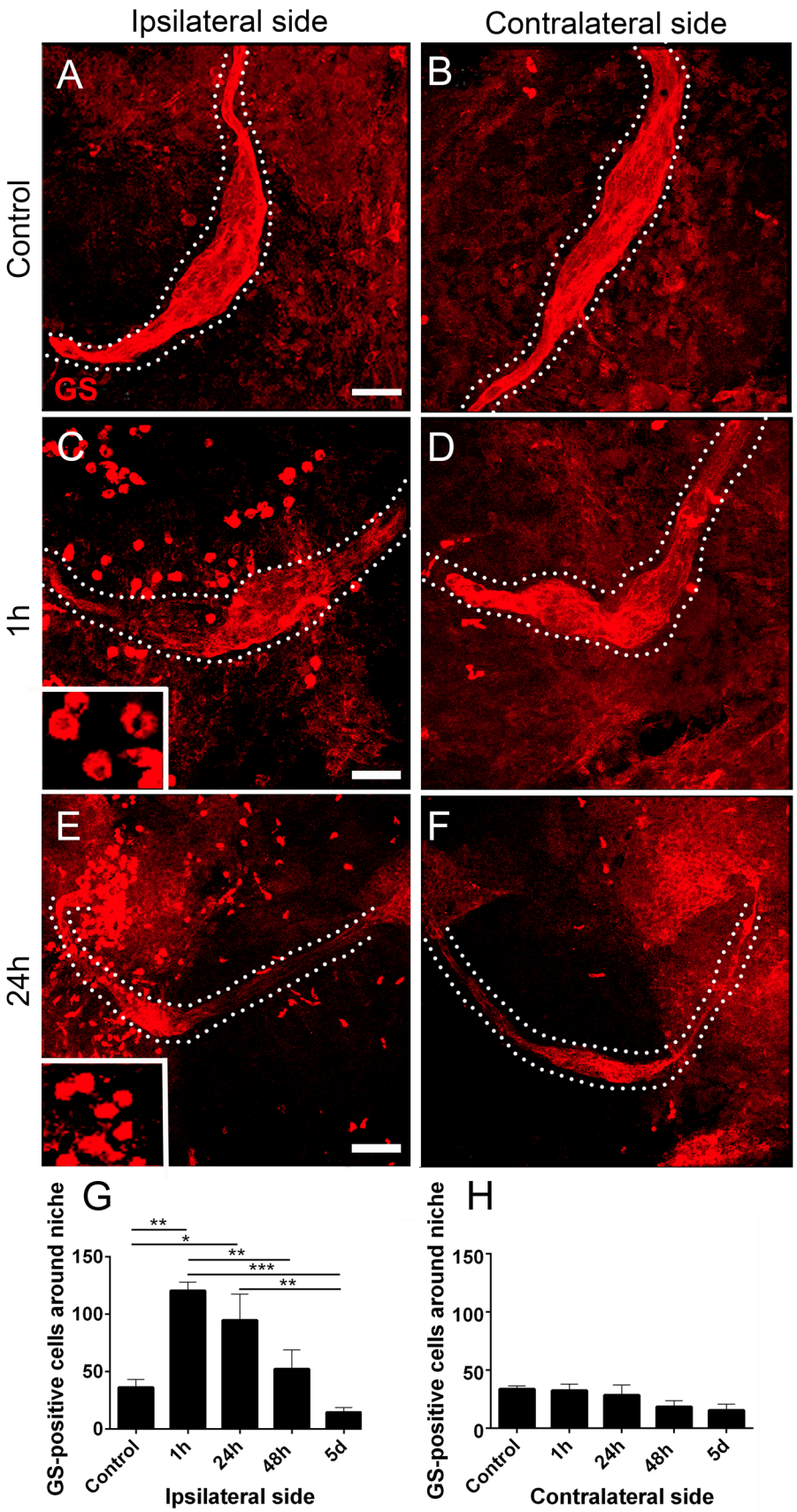

Fig. 8 GS+ cells are observed near the ipsilateral but not the contralateral neurogenic niche after antennular ablation. The niches and streams are delineated by dotted lines. **a**, **b** Controls. **c**, **d** 1 h after lesion. Insets show higher magnification of the granular cells labeled with GS (red). 1 h (**c**) and 24 h (**e**) after ablation there was a significant increase in the number of GS+ cells on the ipsilateral, but not the contralateral, side (**d**, **f**, respectively). **g** The graph shows the number of GS+ cells near the niche on the ipsilateral side. Note that after 24 h the number of cells decreased and the control level was re-established by 5 days after ablation. **h** The contralateral side did not show any statistical differences from the controls at any time point following ablation. * $p < 0{,}05$; ** $p < 0{,}005$; *** $p < 0{,}001$. Scale bars: **a**–**d** 50 µm; **e**, **f** 100 µm

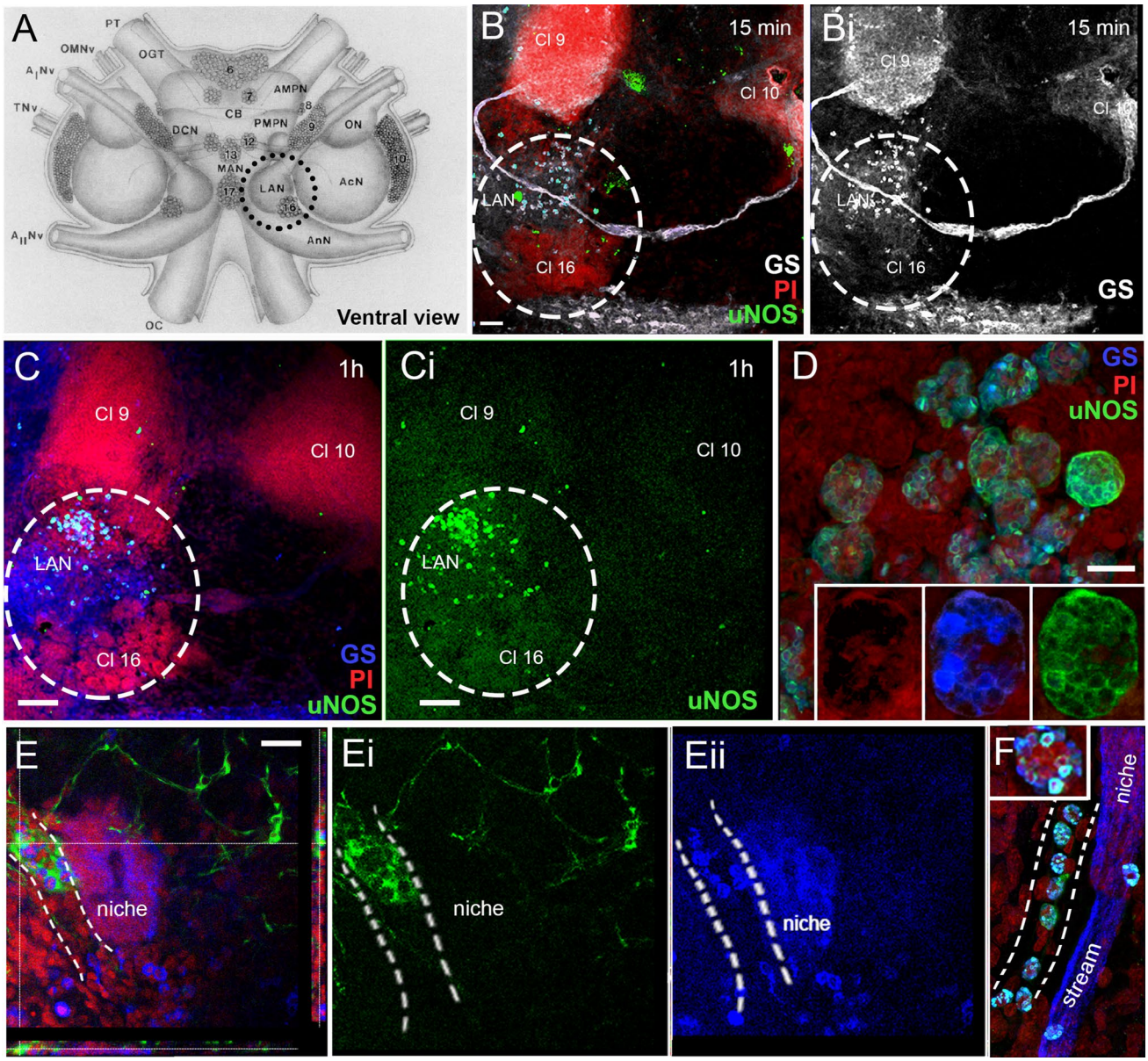

Fig. 9 uNOS + /GS + labeled cells are observed in the lateral antennal neuropil (LAN) after antennular ablation. Schematic diagram of the crayfish brain showing the LAN and cluster 16 (CL16) shown by the black circle (**a**). **b** Immunofluorescence for GS (white) and uNOS (green) of the ipsilateral hemisphere of the crayfish brain showing GS + /uNOS + cells (area circled with white stippling) 15 min after ablation. **bi** The GS channel of the image in B is separated from the other fluorophores. **c** LAN 1 h after ablation. Note that GS (blue) and uNOS (green) colocalize in this region. **ci** Only the uNOS channel of image (**c**). **d** Higher magnification of GS + /uNOS + cells. Insets show cytoplasmic granules labeled with uNOS (green), GS (blue) and PI (red) although the labels appear to be in distinct cellular domains. **e** Confocal microscopy Z-stack image showing a blood vessel (bounded by a dotted line) dorsal to the niche containing GS + /uNOS + cells. **ei** uNOS channel from image (**e**). **eii** GS channel from image (**e**). **f** Another blood vessel dorsal to the niche with GS + blood cells inside. PI (red). Scale bars: **b** 50 µm; **c** 100 µm; **d** 20 µm; **e**, **f** 40 µm. (Image **a** originally from Sandeman et al. 1992, Figure 3B on page 309. Order license # 4653110596087 obtained on 08/20/2019)

that the caliber of blood vessels increased significantly by 24 h after ablation and returned to control dimensions after 48 h, indicating reversible vasodilation (Fig. 11g, h) associated with antennular ablation.

Discussion

In both vertebrates and invertebrates, the production of adult-born neurons is regulated by a variety of factors such as environmental enrichment, diet, circadian signals, serotonin, and nitric oxide (Abrous et al. 2005; Beltz and Benton

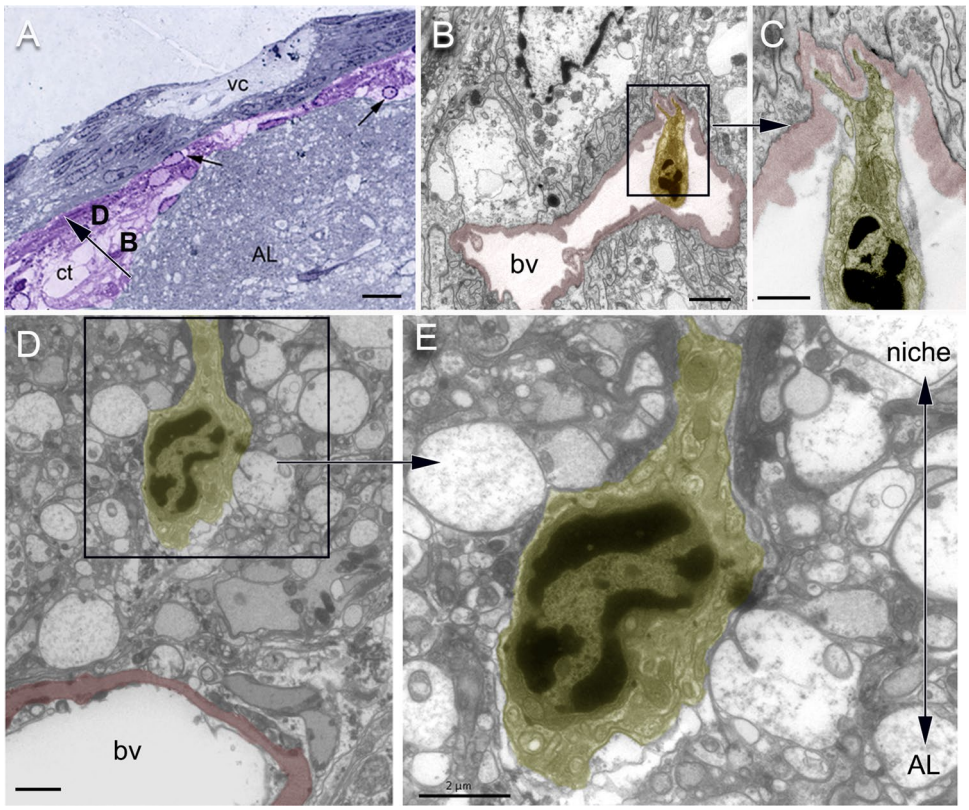

Fig. 10 Hemocytes have cytoplasmic projections on the luminal of blood vessels. **a** Semi-thin section of the neurogenic niche and the vascular cavity (vc) positioned centrally in the neurogenic niche, located on the ventral surface of the accessory lobe (AL). Connective tissue (ct) dorsal to the niche (colorized purple). Note hemocytes (arrows) embedded in the ct. **b** Hemocyte (colorized yellow) within a blood vessel (bv) located dorsal to the niche (not shown) with projections that appear to be inserting into the inner side of the blood vessel lining (**c,** higher magnification of **b**). **d** Hemocyte (colorized yellow) in the surrounding ct, with a cytoplasmic process extending towards the niche. **e** Higher magnification of **d**. Double-headed arrow on the right side of the image indicates the position of the niche and the AL relative to the section. Scale bars: **a** 20 µm; **b** 4 µm; **c**–**e** 2 µm. (Image **a** from Chaves da Silva et al. 2012)

2017; Beltz and Sandeman 2003; Ming and Song 2005). In vertebrates, traumatic brain injury (TBI) may directly affect the proliferation of neural precursor cells (Wang et al. 2016) and induce a complex response that disrupts immune system homeostasis by releasing inflammatory molecules and recruiting immune cells (Carpentier and Palmer 2009). This primary immunological effect of injury may be beneficial, however, it can also be detrimental, since extreme reactivity can trigger excessive inflammatory cascades (Dash et al. 2001; Stoecklein et al. 2012). Some of the delayed responses include neovascularization, impaired brain blood flow, glial cell dysfunction, and cell degeneration, all of which may result in secondary damage (Cernak et al. 2001; Price et al. 2016; Taber et al. 2006).

Here, we performed unilateral antennular ablation in crayfish in order to study the effect of this injury on adult neurogenesis, regions targeted by antennular projections, and the immune and vascular systems. The antennular nerve contains the primary afferents from olfactory receptors on the flagella; all axons from the olfactory sensilla (aesthetascs) project to the OL (Mellon and Munger 1990; Sandeman and Denburg 1976; Schmidt and Ache 1992). Nonaethetasc chemosensory and mechanosensory receptors innervate the LAN and medial antennal neuropil (MAN) (Sandeman and Denburg 1976; Tuchina et al. 2015). Further, the OL contains projections from neurons in CL9 and CL10 into which adult-born neurons are integrated. Our hypothesis therefore was that antennular ablation would directly affect CL9 and CL10 neurons, as well as the neurogenic niche that generates these neurons. Thus, this is an appropriate model to study the relationship between neurodegeneration and neurogenesis in adult crustacean brains.

Four remarkable events are documented here: (1) Unilateral antennular ablation results in a bilateral suppression of neural precursor cell divisions (measured with the S-phase marker BrdU) in the neurogenic niche and in both cell clusters that incorporate adult-born neurons (CL9 and CL10); (2) At least two types of cells (iNOS+and GS+/iNOS−) near the niche were selectively activated following antennular ablation, with the greatest and most rapid change on

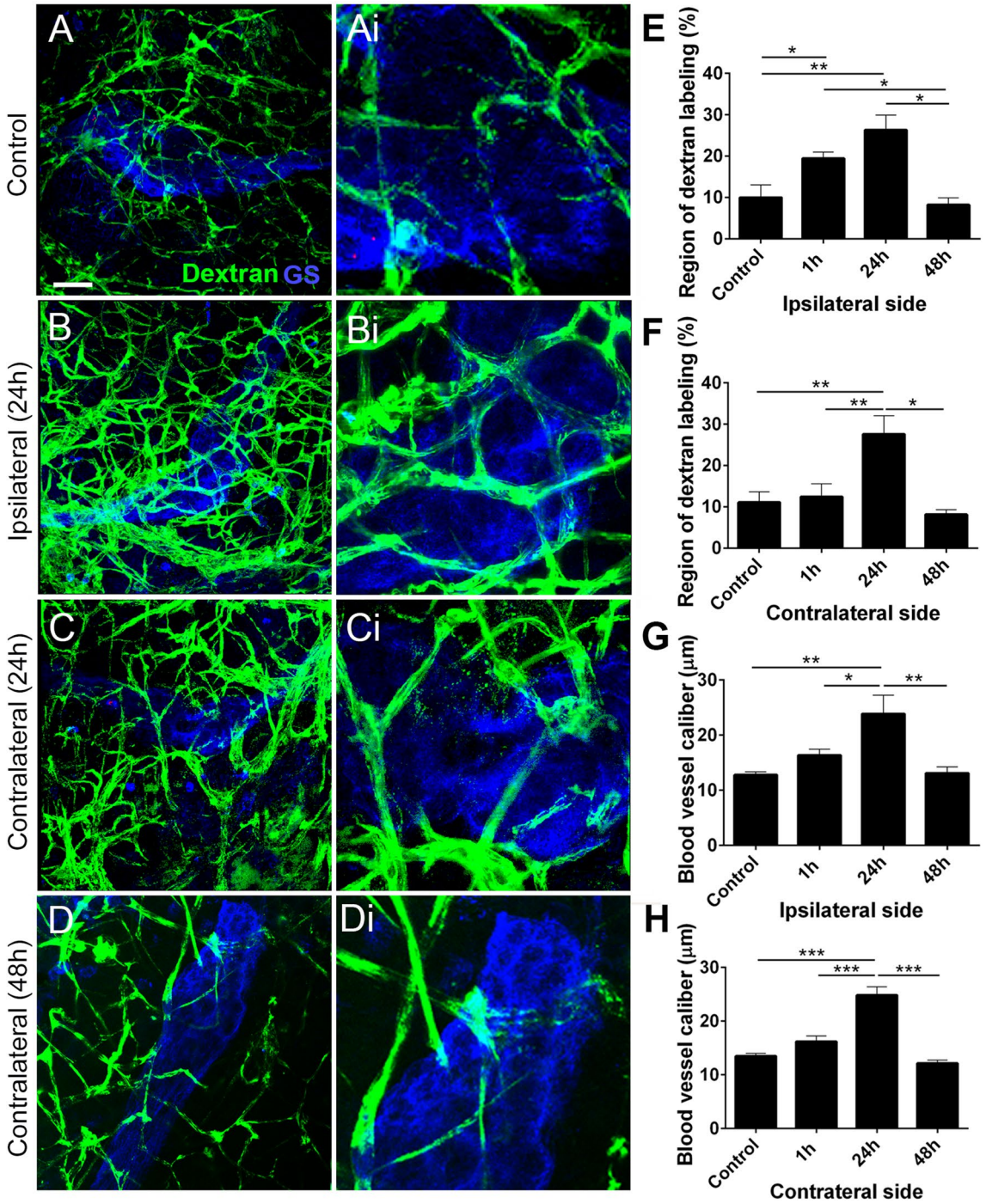

Fig. 11 Blood vessels surrounding the neurogenic niche dilate after antennular ablation. **a**–**d** A vascular net (green) envelops the neurogenic niche (blue). **ai**–**di** Higher magnification images of **a**–**d**. In the controls **a**, **ai**, dextran labeling (green) shows a complex blood vessel network on the ventral surface of the niche. GS+ niche cells are shown in blue. 24 h after ablation, the niche ipsilateral to the antennular damage (B) was more densely surrounded by blood vessels (B,Bi). The vascular network typical of the controls was re-established 48 h after ablation on both sides (D,Di). **e–f** Quantitative analysis of the region occupied by blood vessels, presented as a percentage of the viewing area (1 h, 24 h, and 48 h). **g**–**h** Quantitative analysis of the diameter of the five largest blood vessels surrounding the niches was calculated for the controls and for each time point following antennular ablation (1 h, 24 h, and 48 h). ($n = 5$). *$p < 0{,}05$; **$p < 0{,}005$; ***$p < 0{,}001$. Scale bars: **a**–**d** 50 µm

the side ipsilateral to the ablation; (3) Cells presumed to come from the immune system via the circulation are found in brain regions that receive inputs from the antennule in the first minutes after ablation; and (4) The niche vasculature increases in complexity and blood vessels dilate in response to antennular ablation. These immune and vascular responses are summarized in Fig. 12. Here, unlike in our previous work, the brain was not desheathed during dissection, and therefore, the vasculature attached to the niche was preserved. The advantage is that we could observe the entire niche with its associated vasculature, from ventral to dorsal surfaces and adjacent areas.

Neurogenesis and Traumatic Injury

In vertebrates, it has been shown that neurogenesis can be upregulated in response to different brain insults, including TBI (Dash et al. 2001; Harry 2008; Zheng et al. 2013), and that newly generated neurons can migrate to the site of damage (Richardson et al. 2007). Several studies using different vertebrate models of TBI have demonstrated alterations in adult neurogenesis following injury (Robinson et al. 2016; Shapiro 2017; Wang et al. 2016). Such alterations include increased and/or decreased numbers and survival rates of newborn neurons (Robinson et al. 2016; Wang et al. 2016), as well as aberrant growth and integration of the newborn neurons into existing circuitry (Ibrahim et al. 2016; Robinson et al. 2016; Villasana et al. 2015). However, the severity and/or type and location of injury may impose different impacts on neurogenesis (Shapiro, 2017). For example, it has been shown that mild TBI does not affect neurogenesis with respect to proliferation, migration, or differentiation; moderate TBI may promote proliferation of neural stem cells without increased neuronal production; and severe TBI

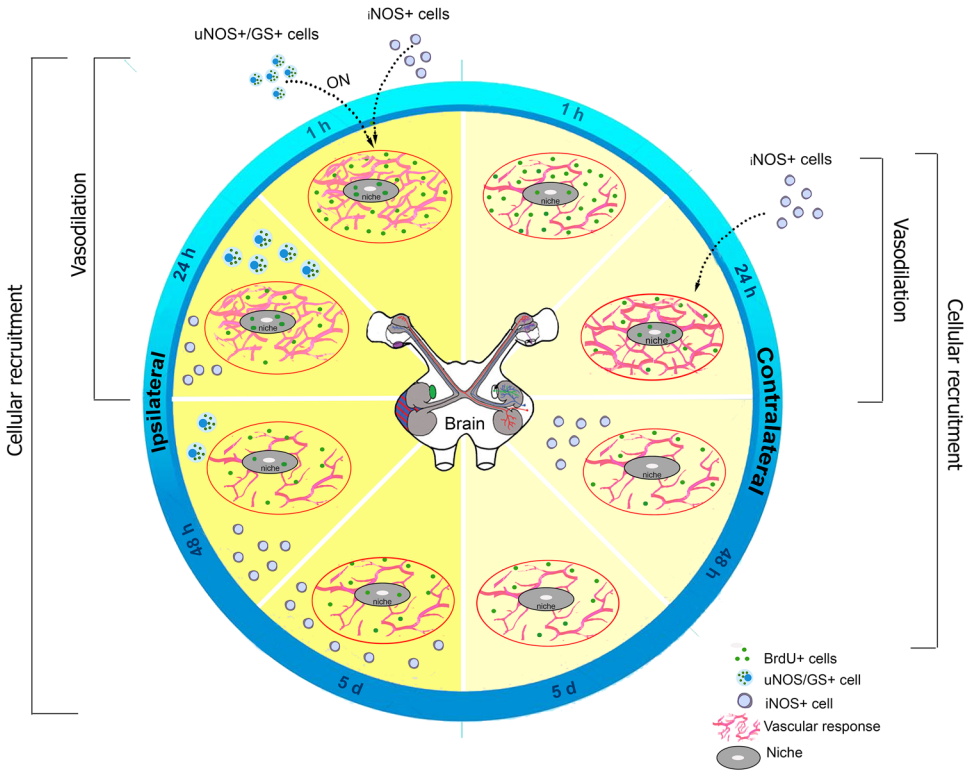

Fig. 12 Immune and vascular responses of the neurogenic niche after antennular ablation. The left side of the image (dark yellow) shows the immune and vascular events associated with the neurogenic niche on the ipsilateral side of the brain. The right side of the diagram (light yellow) shows the side contralateral to the ablation. Every time point after ablation is represented in the blue circle for both sides of the brain (ipsilateral and contralateral). The light blue (on top) represents the acute phase (1 and 24 h) following ablation, and the dark blue (on the bottom) represents the longer-term time points (48 h and 5 days). The scheme of the whole brain is shown in the middle of the circle. *Ipsilateral response* (left side): 1 h after ablation, iNOS+and uNOS + /GS+ cells migrate to the niche (Figs. 5, 8, 9) and the vasculature dilates (Fig. 11). This response persists until 24 h. Forty-eight hours after ablation, the population of GS+ cells is reduced in number (Fig. 8g), and the vascular response returns to control levels (Fig. 11e–g). However, there is still iNOS labeling on the ipsilateral side at 5 days post ablation. *Contralateral response* (right side): the immune and vascular responses begin by 24 h after ablation, but no GS+ cells are seen (Fig. 7h). Forty-eight hours after ablation the region occupied by dextran labeling and the blood vessel diameter are at control levels (Fig. 11f, h). No immune cells are observed by 5 days. The immune and vascular responses are therefore more pronounced on the side ipsilateral to the damage

promotes increased neurogenesis via all of these pathways (Wang et al. 2015).

Among invertebrates, there is very little information on the relationship between neurogenesis and injury. Adult neurogenesis has been analyzed mainly in arthropods, including several species of insects (Cayre et al. 1996) and decapod crustaceans (Chaves da Silva et al. 2015; Schmidt 2007). The relationship between antennule ablation, adult neurogenesis, and NO was examined in juvenile lobsters (*H. americanus*) (Benton et al., 2007). These studies suggested that NOS levels in the olfactory pathway increase after antennular ablation and (either directly or indirectly) suppress neurogenesis among the olfactory projection neurons. However, the neurogenic niche was not the focus of this study. Here, we performed unilateral antennular ablation and then observed decreased proliferation in both brain cell clusters (CL9 and CL10) that incorporate adult-born neurons. Additionally, CL9 was affected first (48 h) on both sides of the brain (Fig. 2), while the response of CL10 was delayed (by 5 days).

It is known that CL9 and CL10 contain the cell bodies of local and projection interneurons, respectively, that project to the OL and accessory lobe (AL) (Fig. 1a; terminology of Sandeman et al. 1992). Further, axons of the CL10 neurons project bilaterally via the olfactory globular tract to neuropil regions in the lateral protocerebrum (Sullivan and Beltz 2001). We hypothesized that antennular ablation would disproportionately affect CL9 because it contains only local interneurons, while CL10 has multiple sources of input that might attenuate or delay the effects of injury. Indeed, in this study antennular ablation resulted in more rapid and severe effects on cell proliferation in CL9 than in CL10.

CL9 and CL10 neurons are generated by a cellular lineage beginning with progenitor cells composing the neurogenic niche (Sullivan et al. 2007a). According to our results, the number of BrdU+ cells in the niche decreased gradually following antennular ablation, which resulted in a significant suppression of proliferation by 48 h that was sustained for at least 5 days (Fig. 3e, g). However, antennular ablation had an even more rapid and severe impact on the number of cells surrounding the niche (Fig. 3f, h). Because these cells require 5–7 days to complete their migration to the proliferation zones (Sullivan et al., 2007a), we suggest that the decreasing number of BrdU+ cells in the niche would not reduce the number of cells in CL9 and CL10 until day 5 of our study, or later. The initial suppression of cell proliferation observed in CL9 and CL10 therefore must be independent of the reduction in niche cell proliferation.

BrdU+ cells may reach the area around the niche via the cerebral artery that carries cells from the anterior proliferation center (Chaves da Silva et al. 2013b). The APC, as mentioned in the Introduction, is a specialized region of the hematopoietic system that may provide neuronal stem cells for adult neurogenesis (and potentially for other functions as well) (Chaves da Silva et al. 2013b; Noonin et al. 2012). Here, we suggest that the BrdU+ cells surrounding the niche (Fig. 3) come from the immune system—potentially the APC—via the circulation, and that their reduced number (at 24 h) may be related to the drop in BrdU+ cells in the niche at 48 h post ablation.

It has been shown that the number of circulating hemocytes can vary and decreases dramatically during an infection (Lorenzon et al. 1999; Persson et al. 1987; Smith and Söderhäll 1983) due to cell recruitment to the site of infection. According to Söderhäll et al. (2003), short-term responses to injury or infection lead to a reduction of free circulating hemocytes followed by compensatory and proportional production of cells, with a continuous release from the HPT and migration to the injury/inflammation site (Johansson et al. 2000; Söderhäll et al. 2003). In the present study, we observed an increase in circulating hemocytes 24 h after ablation (Fig. 6c), perhaps suggesting that by this time point the HPT was activated in order to compensate for recruitment of immune cells to the site of antennular injury (Johansson et al. 2000; Söderhäll et al. 2003). In future studies, it will be interesting to examine THC at earlier time points following antennal ablation, to assess the time course of the anticipated reduction in THC.

A close relationship between the HPT and the generation of neural progenitor cells was demonstrated in adult crayfish by correlating THC with the total number of cells in the neurogenic niche. These experiments showed that manipulating levels of circulating hemocytes resulted in highly predictable and rapid changes in the total number of niche cells (Benton et al. 2014). In the current experiments, the THC was increased by nearly 50% following antennular ablation (Fig. 6c), a change that would have correlated in past studies with a proportional increase in niche cell number. However, we did not observe any changes in the total niche cell count following ablation (Fig. 4). We therefore suggest that although antennular ablation activates the hematopoietic system, resulting in increased THC, that the newly released hemocytes are committed to the site of injury rather than to generating new neurons (as observed by the reduction of BrdU+ cells around and within the niche) (Figs. 12 and 13).

iNOS Labeling Around the Neurogenic Niche

In vertebrates, NO has been described as a neurogenesis modulator, some authors suggest that NO inhibits neurogenesis, while others suggest that NO promotes neurogenesis, particularly under inflammatory conditions (Carreira et al. 2012). The target cell type, NO cell source, reactive status, timing of synthesis, and concentration are major determinants of NO effects (Cárdenas et al. 2005). Our results

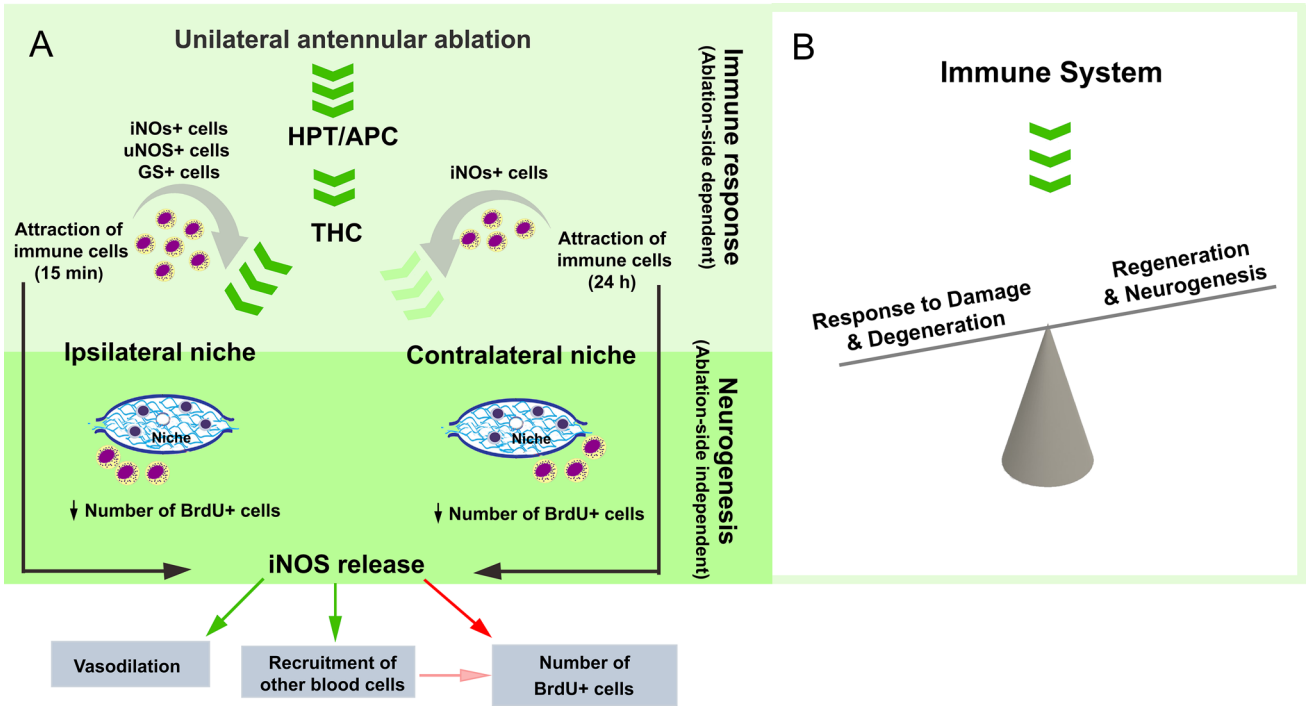

Fig. 13 The crosstalk between neurodegeneration and neurogenesis: What is the effect of unilateral ablation on neurogenesis and the immune response in adult crayfish? **a** The immune response (light green square) is ablation-side dependent in the first few hours (15 min) after lesion: the unilateral antennular ablation activates (green arrow) the hematopoietic tissue (HPT/APC), inducing an increase in total hemocyte count (THC). This response is correlated with an increase (dark green arrowheads) in the number of iNOS, uNOS, and GS+cells (gray curved arrow) around the neurogenic niche on the ipsilateral, but not on the contralateral side (15 min) after ablation. Once these cells are activated, they may contribute to releasing of nitric oxide (NO), which is hypothesized to cause vasodilation and recruitment of other blood cells. 24 h after ablation, an immune response (gray curved arrow) was observed on the contralateral side, although this was not as intense as on the ipsilateral side (light green arrowheads). The dark green square (bottom) shows the ablation effects on neurogenesis, which is ablation-side independent. A decrease in BrdU+cells in and around the niche was observed on both sides of the brain (Fig. 3e, f), however, with no significant changes in the total number of cells in the niche (Fig. 4). **b** It is proposed that the immune response to antennular ablation shifts the balance such that newly produced hemocytes (immune system), are recruited preferentially to the site of *Damage & Degeneration* (left side) rather than to R*egeneration & Neurogenesis* (right side)

suggest that the NO system also exerts powerful control over the formation of new neurons in invertebrates.

In the lobster *H. americanus*, it has already been shown that NO participates in the neural response to injury. NOS levels increase after antennular ablation in the olfactory pathway and are associated with a suppression of neurogenesis among the olfactory projection neurons. The direct involvement of NO in neurogenesis was demonstrated by using the NO donor SNAP and NOS inhibitor L-NAA to manipulate NO levels and examine the influence on neural proliferation (BrdU+profiles) (Benton et al. 2007). This was also confirmed by preliminary results using L-NAA obtained in adult *P. clarkii* (data not shown). Here, we observed three important aspects of iNOS immunoreactivity: (1) a time-dependent increase in iNOS expression around the niche and in the vascular cavity after lesion (Fig. 5); (2) the lateralized expression of iNOS 1 h after ablation in cells in the vicinity of the niche (Fig. 7); (3) a lack of GS labeling in iNOS+ cells, but not in uNOS+cells. Considering that iNOS was expressed bilaterally in and around the niche by 24 h after ablation and that this correlated with the decreased numbers of BrdU+cells surrounding the niche (Fig. 3), we hypothesize that iNOS expression may have suppressed the proliferation of neural progenitors in the niche by decreasing the number of BrdU+cells available in the vicinity of the niche. It is not known whether immune cells go through S-phase prior to integrating into the niche, where the cell cycle may be completed, although the current data allude to this possibility.

According to our results, the peak in bilateral iNOS labeling was seen between 24 and 48 h after ablation (Fig. 5), which is the same time frame for the observed vascular dilation (Fig. 11). However, by 48 h, the vascular response in the neurogenic niche returned to that seen in the control animals, although intense iNOS labeling in cells around the niche persisted for at least 5 days and was particularly pronounced on

the side ipsilateral to the ablation, although NO levels were not quantified. These results suggest that (1) active molecules in addition to NO are released by the immune cells or in response to NO after antennular ablation; or (2) because NO rapidly diffuses (Kelm 1999), its action may have lessened over time, as appears to have occurred with the vasculature in both sides of the brain. These features related to NO action may contribute to the specific response of the brain vasculature after ablation. In the future, we will examine the response of the vasculature to antennal ablation in other tissues/locations apart from the brain, to determine whether the vascular response extends beyond the brain regions directly affected by cutting the antennule. Interestingly, GS+ cells found near the neurogenic niche following ablation co-labeled for uNOS (Fig. 9d) (an antibody that detects the three isoforms of NOS) but not for iNOS. This indicates that the production of NO by GS+ cells did not occur as a result of iNOS activity. It is possible that these cells produce the constitutive isoform of NOS via endothelial and/or neuronal NOS (eNOS or nNOS, respectively), which in vertebrates are related, among other functions, with positive regulation of neurogenesis (Jin et al. 2017). According to these data, we believe that at least two types of cells were recruited to the niche acutely after injury: (1) iNOS+ cells, which may induce inflammatory processes (Chaves da Silva et al. 2010, 2012), and (2) uNOS + /GS+ cells, whose functions in this system are not known. It is important to note that, unlike the BrdU experiments that show the accumulated labeling over a 24-h period, the iNOS and GS labeling represent only a snapshot at a specific time. Therefore, dynamic changes in the synthesis of these molecules during the sampling period may not have been detected.

LAN and Cluster 16

While the olfactory (aesthetasc) afferents in the antennular nerve project exclusively to the OL, mechanoreceptors, statocysts, and nonaesthetasc chemoreceptors project to the LAN (Blaustein et al. 1988; Schmidt and Ache 1996a). Further, CL16 contains cell bodies that project to both the OL and LAN (Arbas et al. 1988). The antennular nerve, OL, LAN, and Cluster 16 therefore comprise a major part of the neural pathway involving the antennules.

Here, we observed that the ipsilateral LAN and CL16 were responsive to the injury unilaterally since iNOS+ and uNOS+ circulating cells were associated with those regions 15 min after ablation. Because the antennular nerve is composed of fibers projecting to the LAN, the ablation procedure was adequate to trigger an inflammatory response by activating circulating cells in both the LAN and CL16. These results suggest that signaling molecules were retrogradely transported to the neuronal somata in CL16 in the first few minutes after ablation, even though there were no gross morphological changes observed in the cellular/brain structure.

These data therefore suggest that within minutes of antennular ablation, the targets of the antennular nerve (OL and LAN) begin to respond to the injury, as well as those neurons projecting to these regions (CL9, CL10, CL16) that may lose their innervation or post-synaptic target as a result of the ablation. While the current work has described the short-term effects (15 min—5 days) of antennular ablation on these regions, it will be interesting in future studies to follow the progression of this injury response on a longer time scale, as the OL is reconstituted and adult neurogenesis re-establishes the numbers of neurons in CL9 and CL10, as previously demonstrated by (Sandeman et al. 1998).

Conclusions

Here, we suggest that hemocytes play a key role in both neurodegeneration and neurogenesis: in physiological conditions, they maintain the number of niche cells and promote neurogenesis, while in pathological conditions (neurodegeneration), they appear to be involved in NO release and vascular responses associated with the neurogenic niche, as summarized in Fig. 13.

Our data suggest that these processes are co-regulated, and that neural damage provokes an immediate suppression of neurogenesis in both the neurogenic niche and in CL9 and CL10 where adult-born neurons differentiate. Because hemocytes in crayfish are a source of neural progenitor cells as well as agents of immune function, we suggest a balance between these sometimes competing roles (Fig. 13). Our results indicate that tissue damage is the key factor in the deployment of hemocytes for injury and repair functions, rather than for neurogenesis. Further clarity regarding the role of the immune system will come with a greater understanding of the specific hemocyte types and signaling mechanisms that participate in neurogenesis and repair.

Acknowledgements This work was supported by the Coordenação de Aperfeiçoamento de Pessoal de Nível Superior (CAPES/Brazil), Grant number 8698-11-2 (to P. Chaves da Silva), Conselho Nacional de Desenvolvimento Científico e Tecnológico (CNPq/Brazil), Grant number 304648/2014-0 (to S. Allodi), Fundação Carlos Chagas Filho de Apoio à Pesquisa do Estado do Rio de Janeiro (FAPERJ/Brazil), Grant number E26/202.762/2017 (to S. Allodi), and U.S. National Science Foundation, Grant numbers IOS-1121345 and IOS-1656103 (to B. Beltz). We are grateful to the Rudolf Barth Electron Microscopy Platform of the Oswaldo Cruz Institute/Fiocruz for the electron microscopy facilities.

Author Contributions PGCS was involved in experimental design, execution, and analysis of all experiments. KH performed the studies described in Figs. 4 and 6c. JLB was involved in experimental design and assisted with some experiments. BSB helped with planning and

analysis of experiments and was directly involved in the niche cell and total hemocyte counts. SA contributed to data analysis and overall project planning. PGCS composed the first draft of the manuscript, which was read critically and revised by all authors.

Compliance with Ethical Standards

Conflict of interest Authors declare that they have no conflict of interest.

References

Abrous DN, Koehl M, Le Moal M (2005) Adult neurogenesis: from precursors to network and physiology. Physiol Rev 85:523–569. https://doi.org/10.1152/physrev.00055.2003

Arbas EA, Humphreys CJ, Ache BW (1988) Morphology and physiological properties of interneurons and olfactory midbrain of the crayfish. J Comp Physiol A 164:231–241. https://doi.org/10.1007/BF00603953

Beckman JS, Koppenol WH (1996) Nitric oxide, superoxide, and peroxynitrite: the good, the bad, and ugly. Am J Physiol 271:1424–1437. https://doi.org/10.1152/ajpcell.1996.271.5.C1424

Beltz BS, Benton JL (2017) From blood to brain: adult-born neurons in the crayfish brain are the progeny of cells generated by the immune system. Front Neurosci 11:662. https://doi.org/10.3389/fnins.2017.00662

Beltz BS, Sandeman DC (2003) Regulation of life-long neurogenesis in the decapod crustacean brain. Arthropod Struct Dev 32:39–60. https://doi.org/10.1016/S1467-8039(03)00038-0

Benton JL, Sandeman DC, Beltz BS (2007) Nitric oxide in the crustacean brain: regulation of neurogenesis and morphogenesis in the developing olfactory pathway. Dev Dyn 236:3047–3060. https://doi.org/10.1002/dvdy.21340

Benton JL, Zhang Y, Kirkhart CR, Sandeman DC, Beltz BS (2011) Primary neuronal precursors in adult crayfish brain: replenishment from a non-neuronal source. BMC Neurosci 12:53. https://doi.org/10.1186/1471-2202-12-53

Benton JL, Chaves da Silva PG, Sandeman DC, Beltz BS (2013) First-generation neuronal precursors in the crayfish brain are not self-renewing. Int J Dev Neurosci 31:657–666. https://doi.org/10.1016/j.ijdevneu.2012.11.010

Benton JL, Kery R, Li J, Noonin C, Söderhäll I, Beltz BS (2014) Cells from the immune system generate adult-born neurons in crayfish. Dev Cell 30:322–333. https://doi.org/10.1016/j.devcel.2014.06.016

Blaustein DN, Derby CD, Simmons RB, Beall AC (1988) Structure of the brain and medulla terminalis of the spiny lobster *Panulirus argus* and the crayfish *Procambarus clarkii*, with an emphasis on olfactory centers. J Crustac Biol 8:493–519. https://doi.org/10.1163/193724088X00341

Brenneis G, Beltz BS (2019) Adult neurogenesis in crayfish: origin, expansion and migration of neural progenitor lineages in a pseudostratified neuroepithelium. J Comp Neurol. https://doi.org/10.1002/cne.24820

Calabrese V, Mancuso C, Calvani M, Rizzarelli E, Butterfield DA, Giuffrida Stella AM (2007) Nitric oxide in the central nervous system: neuroprotection versus neurotoxicity. Nat Rev Neurosci 8:766–775. https://doi.org/10.1038/nrn2214

Cárdenas A, Moro MA, Hurtado O, Leza JC, Lizasoain I (2005) Dual role of nitric oxide in adult neurogenesis. Brain Res Rev 50:1–6. https://doi.org/10.1016/j.brainresrev.2005.03.006

Carpentier PA, Palmer TD (2009) Immune influence on adult neural stem cell regulation and function. Neuron 64:79–92. https://doi.org/10.1016/j.neuron.2009.08.038

Carreira BP, Carvalho CM, Araújo IM (2012) Regulation of injury-induced neurogenesis by nitric oxide. Stem Cells Int 2012:15. https://doi.org/10.1155/2012/895659

Cayre M, Strambi C, Charpin P, Augier R, Meyer MR, Edwards JS, Strambi A (1996) Neurogenesis in adult insect mushroom bodies. J Comp Neurol 22:300–310. https://doi.org/10.1002/(SICI)1096-9861(19960722)371:2%3c300:AID-CNE9%3e3.0.CO;2-6

Cernak I, Wang Z, Jiang J, Bian X, Savic J (2001) Ultrastructural and functional characteristics of blast injury-induced neurotrauma. J Trauma 50:695–706. https://doi.org/10.1097/00005373-200104000-00017

Chaves da Silva PG, de Barros CM, Lima FRS, Biancalana A, Martinez AMB, Allodi S (2010) Identity of the cells recruited to a lesion in the central nervous system of a decapod crustacean. Cell Tissue Res 342:179–189. https://doi.org/10.1007/s00441-010-1045-x

Chaves da Silva PG, Benton JL, Beltz BS, Allodi S (2012) Adult neurogenesis: ultrastructure of a neurogenic niche and neurovascular relationships. PLoS ONE 7(6):e39267. https://doi.org/10.1371/journal.pone.0039267

Chaves da Silva PG, Benton JL, Sandeman DC, Beltz BS (2013a) Adult neurogenesis in the crayfish brain: the hematopoietic anterior proliferation center has direct access to the brain and stem cell niche. Stem Cells Dev 22:1027–1041. https://doi.org/10.1089/scd.2012.0583

Chaves da Silva PG, Corrêa CL, de Carvalho SL, Allodi S (2013b) The crustacean central nervous system in focus: subacute neurodegeneration induces a specific innate immune response. PLoS ONE 8:e80896. https://doi.org/10.1371/journal.pone.0080896

Chaves da Silva PG, Santos de Abreu I, Cavalcante LA, de Barros CM, Allodi S (2015) Role of hemocytes in invertebrate adult neurogenesis and brain repair. Invertebr Surviv J 12:142–154

Dash PK, Mach SA, Moore AN (2001) Enhanced neurogenesis in the rodent hippocampus following traumatic brain injury. J Neurosci Res 63:313–319. https://doi.org/10.1002/1097-4547(20010215)63:4%3c313:AID-JNR1025%3e3.0.CO;2-4

Doetsch F, Caillé I, Lim DA, García-Verdugo JM, Alvarez-Buylla A (1999) Subventricular zone astrocytes are neural stem cells in the adult mammalian brain. Cell 97:703–716

Harry GJ (2008) Neurogenesis and brain repair. In: Neuroimmune pharmacology. Springer, Boston, pp. 445–462. https://doi.org/10.1007/978-0-387-72573-4_32.

Harzsch S, Krieger J (2018) Crustacean olfactory systems: a comparative review and a crustacean perspective on olfaction in insects. Prog Neurobiol 161:23–60. https://doi.org/10.1016/j.pneurobio.2017.11.005

Hillyer JF, Estévez-Lao TY (2010) Nitric oxide is an essential component of the hemocyte-mediated mosquito immune response against bacteria. Dev Comp Immunol 34:141–149. https://doi.org/10.1016/j.dci.2009.08.014

Horgusluoglu E, Nudelman K, Nho K, Saykin AJ (2017) Adult neurogenesis and neurodegenerative diseases: a systems biology perspective. Am J Med Genet Part B 174:93–112. https://doi.org/10.1002/ajmg.b.32429

Howes EA, Chain BM, Smith PJS, Treherne JE (1987) Blood cells contribute to glial repair in an insect. Tissue Cell 19:877–880. https://doi.org/10.1016/0040-8166(87)90026-7

Ibrahim S, Hu W, Wang X, Gao X, He C, Chen J (2016) Traumatic brain injury causes aberrant migration of adult-born neurons in the hippocampus. Sci Rep 6:21793. https://doi.org/10.1038/srep21793

Jin X, Yu Z-F, Chen F, Lu G-X, Ding X-Y, Xie L-J, Sun J-T (2017) Neuronal nitric oxide synthase in neural stem cells induces

neuronal fate commitment via the inhibition of histone deacetylase 2. Front Cell Neurosci 11:66. https://doi.org/10.3389/fncel.2017.00066

Johansson KU, Carlberg M (1994) NADPH-diaphorase histochemistry and nitric oxide synthase activity in deutocerebrum of the crayfish, *Pacifastacus leniusculus* (Crustacea, Decapoda). Brain Res 649:36–42

Johansson MW, Keyser P, Sritunyalucksana K, Söderhäll K (2000) Crustacean haemocytes and haematopoiesis. Aquaculture 191:45–52. https://doi.org/10.1016/S0044-8486(00)00418-X

Kelm M (1999) Nitric oxide metabolism and breakdown. Biochim Biophys Acta 1411:273–289. https://doi.org/10.1016/S0005-2728(99)00020-1

Leiter O, Kempermann G, Walker TL (2016) A common language: how neuroimmunological cross talk regulates adult hippocampal neurogenesis. Stem Cells Int 2016:1–13. https://doi.org/10.1155/2016/1681590

Lin X, Söderhäll I (2011) Crustacean hematopoiesis and the astakine cytokines. Blood 117:6417–6424. https://doi.org/10.1182/blood-2010-11-320614

Lind M, Hayes A, Caprnda M, Petrovic D, Rodrigo L, Kruzliak P, Zulli A (2017) Inducible nitric oxide synthase: good or bad? Biomed Pharmacother 93:370–375. https://doi.org/10.1016/j.biopha.2017.06.036

Lorenzon S, de Guarrini S, Smith VJ, Ferrero EA (1999) Effects of LPS injection on circulating haemocytes in crustaceans in vivo. Fish Shellfish Immunol 9:31–50. https://doi.org/10.1006/FSIM.1998.0168

Mellon D, Munger SD (1990) Nontopographic projection of olfactory sensory neurons in the crayfish brain. J Comp Neurol 296:253–262. https://doi.org/10.1002/cne.902960205

Ming G, Song H (2005) Adult neurogenesis in the mammalian central nervous system. Annu Rev Neurosci 28:223–250. https://doi.org/10.1146/annurev.neuro.28.051804.101459

Noonin C, Lin X, Jiravanichpaisal P, Söderhäll K, Söderhäll I (2012) Invertebrate hematopoiesis: an anterior proliferation center as a link between the hematopoietic tissue and the brain. Stem Cells Dev 21:3173–3186. https://doi.org/10.1089/scd.2012.0077

Novas A, Cao A, Barcia R, Ramos-Martinez JI (2004) Nitric oxide release by hemocytes of the mussel *Mytilus galloprovincialis* Lmk was provoked by interleukin-2 but not by lipopolysaccharide. Int J Biochem Cell Biol 36:390–394

Palumbo A (2005) Nitric oxide in marine invertebrates: a comparative perspective. Comp Biochem Physiol Part A 142:241–248. https://doi.org/10.1016/j.cbpb.2005.05.043

Pathania M, Yan LD, Bordey A (2010) A symphony of signals conducts early and late stages of adult neurogenesis. Neuropharmacology 58:865–876. https://doi.org/10.1016/j.neuropharm.2010.01.010

Persson M, Cerenius L, Söderhäll K (1987) The influence of haemocyte number on the resistance of the freshwater crayfish, *Pacifastacus leniusculus* Dana, to the parasitic fungus *Aphanomyces astaci*. J Fish Dis 10:471–477. https://doi.org/10.1111/j.1365-2761.1987.tb01098.x

Price L, Wilson C, Grant G (2016) Blood–brain barrier pathophysiology following traumatic brain injury, translational research in traumatic brain injury. CRC Press, Boca Raton

Richardson RM, Sun D, Bullock MR (2007) Neurogenesis after traumatic brain injury. Neurosurg Clin N Am 18:169–181. https://doi.org/10.1016/J.NEC.2006.10.007

Robinson C, Apgar C, Shapiro LA (2016) Astrocyte Hypertrophy contributes to aberrant neurogenesis after traumatic brain injury. Neural Plast 2016:1347987. https://doi.org/10.1155/2016/1347987

Sandeman DC, Denburg JL (1976) The central projections of chemoreceptor axons in the crayfish revealed by axoplasmic transport. Brain Res 115:492–496

Sandeman D, Sandeman R, Derby C, Schmidt M (1992) Morphology of the brain of crayfish, crabs, and spiny lobsters: a common nomenclature for homologous structures. Biol Bull 183:304–326. https://doi.org/10.2307/1542217

Sandeman R, Clarke D, Sandeman D, Manly M (1998) Growth-related and antennular amputation-induced changes in the olfactory centers of crayfish brain. J Neurosci 18:6195–6206

Schachtner J, Schmidt M, Homberg U (2005) Organization and evolutionary trends of primary olfactory brain centers in Tetraconata (Crustacea + Hexapoda). Arthropod Struct Dev 34:257–299. https://doi.org/10.1016/j.asd.2005.04.003

Schmidt M (2007) The Olfactory pathway of decapod crustaceans-an invertebrate model for life-long neurogenesis. Chem Sens 32:365–384. https://doi.org/10.1093/chemse/bjm008

Schmidt M, Ache BW (1992) Antennular projections to the midbrain of the spiny lobster. II. Sensory innervation of the olfactory lobe. J Comp Neurol 318:291–303. https://doi.org/10.1002/cne.903180306

Schmidt M, Ache BW (1996a) Processing of antennular input in the brain of the spiny lobster, *Panulirus argus*. II. The olfactory pathway. J Comp Physiol A 178:605–628. https://doi.org/10.1007/BF00227375

Schmidt M, Ache BW (1996b) Processing of antennular input in the brain of the spiny lobster, *Panulirus argus* I non–olfactory chemosensory and mechanosensory pathway of the lateral and median antennular neuropils. J Comp Physiol A 178:579–604

Schmidt M, Van Ekeris L, Ache BW (1992) Antennular projections to the midbrain of the spiny lobster. I. sensory innervation of the lateral and medial antennular neuropils. J Comp Neurol 318:277–290

Shapiro LA (2017) Altered hippocampal neurogenesis during the first 7 days after a fluid percussion traumatic brain injury. Cell Transpl 26:1314–1318. https://doi.org/10.1177/0963689717714099

Smith V, Söderhäll K (1983) Induction of degranulation and lysis of haemocytes in the freshwater crayfish, *Astacus astacus* by components of the prophenoloxidase activating system in vitro. Cell Tissue Res 233:295–303. https://doi.org/10.1007/BF00238297

Smith PJS, Leech CA, Treherne JE (1984) Glial repair in an insect central nervous system: effects of selective glial disruption. J Neurosci 4:2698–2711. https://doi.org/10.1523/JNEUROSCI.04-11-02698.1984

Smith PJ, Howes EA, Treherne JE (1987) Mechanisms of glial regeneration in an insect central nervous system. J Exp Biol 132:59–78. https://doi.org/10.1.1.553.9453

Smith LK, White CW, Villeda SA (2018) The systemic environment: at the interface of aging and adult neurogenesis. Cell Tissue Res 371:105–113. https://doi.org/10.1007/s00441-017-2715-8

Söderhäll K, Smith V, Johansson M (1986) Exocytosis and uptake of bacteria by isolated haemocyte populations of two crustaceans: evidence for cellular co-operation in the defence reactions of arthropods. Cell Tissue Res 245:43–49. https://doi.org/10.1007/BF00218085

Söderhäll I, Bangyeekhun E, Mayo S, Söderhäll K (2003) Hemocyte production and maturation in an invertebrate animal; proliferation and gene expression in hematopoietic stem cells of *Pacifastacus leniusculus*. Dev Comp Immunol 27:661–672

Stoecklein VM, Osuka A, Lederer JA (2012) Trauma equals danger-damage control by the immune system. J Leukoc Biol 92:539–551. https://doi.org/10.1189/jlb.0212072

Sullivan JM, Beltz BS (2001) Neural pathways connecting the deutocerebrum and lateral protocerebrum in the brains of decapod crustaceans. J Comp Neurol 441:9–22. https://doi.org/10.1002/cne.1394

Sullivan JM, Beltz BS (2005) Integration and segregation of inputs to higher-order neuropils of the crayfish brain. J Comp Neurol 481:118–126. https://doi.org/10.1002/cne.20346

Sullivan JM, Sandeman DC, Benton JL, Beltz BS (2007a) Adult neurogenesis and cell cycle regulation in the crustacean olfactory pathway: from glial precursors to differentiated neurons. J Mol Histol 38:527–542. https://doi.org/10.1007/s10735-007-9112-7

Sullivan JM, Benton JL, Sandeman DC, Beltz BS (2007b) Adult neurogenesis: a common strategy across diverse species. J Comp Neurol 500:574–584. https://doi.org/10.1002/cne.21187

Taber KH, Warden DL, Hurley RA (2006) Blast-related traumatic brain injury: what is known? J Neuropsychiatry Clin Neurosci 18:141–145. https://doi.org/10.1176/jnp.2006.18.2.141

Tota B, Wang T (2005) Nitric oxide: comparative aspects of respiratory and cardiovascular homeostasis. Comp Biochem Physiol Part A 142:99–101. https://doi.org/10.1016/j.cbpa.2005.08.026

Tuchina O, Koczan S, Harzsch S, Rybak J, Wolff G, Strausfeld N, Hansson B (2015) Central projections of antennular chemosensory and mechanosensory afferents in the brain of the terrestrial hermit crab (*Coenobita clypeatus*; Coenobitidae, Anomura). Front Neuroanat 9:94–107. https://doi.org/10.3389/fnana.2015.00094

Villasana LE, Kim KN, Westbrook GL, Schnell E (2015) Functional integration of adult-born hippocampal neurons after traumatic brain injury. eNeuro. https://doi.org/10.1523/ENEURO.0056-15.2015.

Wang H-K, Lee Y-C, Huang C-Y, Liliang P-C, Lu K, Chen H-J, Li Y-C, Tsai K (2015) Traumatic brain injury causes frontotemporal dementia and DP-43 proteolysis. Neuroscience 300:94–103. https://doi.org/10.1016/j.neuroscience.2015.05.013

Wang X, Gao X, Michalski S, Zhao S, Chen J (2016) Traumatic brain injury severity affects neurogenesis in adult mouse hippocampus. J Neurotrauma 33:721–733. https://doi.org/10.1089/neu.2015.4097

Yoshino M, Kondoh Y, Hisada M (1983) Projection of statocyst sensory neurons associated with crescent hairs in the crayfish *Procambarus clarkii* girard. Cell Tissue Res 230:37–48

Zhang Y, Allodi S, Sandeman DC, Beltz BS (2009) Adult neurogenesis in the crayfish brain: proliferation, migration, and possible origin of precursor cells. Dev Neurobiol 69:415–436. https://doi.org/10.1002/dneu.20717

Zheng W, ZhuGe Q, Zhong M, Chen G, Shao B, Wang H, Mao X, Xie L, Jin K (2013) Neurogenesis in adult human brain after traumatic brain injury. J Neurotrauma 30:1872–1880. https://doi.org/10.1089/neu.2010.1579

Ziv Y, Schwartz M (2008) Orchestrating brain-cell renewal: the role of immune cells in adult neurogenesis in health and disease. Trends Mol Med 14:471–478